

# Non-Linear Finite Element Optimization for Inelastic Buckling Modelling of Smooth Rebars

Di Sarno, Luigi,

*Senior Lecturer in Structural and Earthquake Engineering, Institute for Risk and Uncertainty, School of Engineering,  
University of Liverpool, Liverpool, UK. Email address: [Luigi.Di-sarno@liverpool.ac.uk](mailto:Luigi.Di-sarno@liverpool.ac.uk)*

Pugliese, Francesco,

*PhD Candidate in Seismic Analysis and Risk Assessment, Institute for Risk and Uncertainty, School of Engineering,  
University of Liverpool, Liverpool, UK. Email address: [Francesco.Pugliese@liverpool.ac.uk](mailto:Francesco.Pugliese@liverpool.ac.uk)*

and

De Risi, Raffaele,

*Lecturer in Civil Engineering, Department of Civil Engineering, University of Bristol, Bristol, UK. Email address:  
[raffaele.derisi@bristol.ac.uk](mailto:raffaele.derisi@bristol.ac.uk)*

All authors contributed equally to the research;

**Abstract:** This paper presents an optimization methodology to simulate the monotonic and cyclic response of steel reinforcement smooth bars when subjected to inelastic buckling. A finite element (FE) model of steel rebars, based on non-linear fibre sections and an initial geometrical imperfection, is adopted. The multi-step optimization proposed herein to identify the main parameters of the material constitutive models is based on genetic algorithms (GA) and Bayesian model updating. The methodology consists of comparing available experimental tests from literature with the corresponding numerical results. New empirical relationships and probabilistic distributions of the optimized model parameters, such as post-yielding hardening ratio, isotropic hardening in compression and tension, plus initial curvature, are presented. Finally, utilizing both the GA-based and Bayesian-based calibration, an improvement of an existing analytical model for inelastic buckling of smooth steel rebars is proposed. Such analytical modelling can be efficient and reliable for future building codes and assessment guidelines for existing buildings.

## 1. INTRODUCTION

Many existing reinforced concrete (RC) buildings and bridges were designed in the 60s and 70s according to obsolete non-seismic codes. Such structures were reinforced with “smooth” rebars (e.g., Arani et al., 2013; Arani et al., 2014; Abbiati et al., 2015; Melo et al., 2015; De Risi et al., 2017) and using poor seismic details (e.g., hook anchoring, short bar lap splice, large stirrups spacing, (e.g., Fabbrocino et al., 2008-Part-I; Fabbrocino et al., 2008-Part II; Verderame et al., 2009-Part I; Verderame et al., 2009-Part II)). As a consequence, the global response of RC structures may completely change as RC components could fail under the combined action flexure and shear. Recent earthquakes exemplified the vulnerability of such RC structures, even for low-intensity ground motions. Thus, it is imperative to comprehensively investigate the seismic performance of existing RC structures with smooth rebars. Most of the critical deficiencies of such RC structures could be attributed to the exposure to aggressive environments over their lifetime (e.g., Di Sarno and Pugliese, 2020a-2020b, among others), which have triggered the phenomenon of deterioration (i.e., corrosion). The ageing effects resulted in cracking and spalling of the concrete cover, as well as deterioration of the bond strength between steel reinforcement and concrete (Robushi et al., 2020). Bond deterioration and cover spalling may lead to buckling of longitudinal bars when the structure is subjected to seismic

46 loads. Such a phenomenon is often neglected when analysing columns and shear walls, especially in  
47 the critical regions at the structural components. As a result, the behaviour of RC elements and,  
48 therefore, the global capacity of structures may be overestimated to the actual strength, ductility and,  
49 in turn, energy dissipation capacity.

50 Thus, the choice of an accurate constitutive model for smooth steel reinforcement plays a significant  
51 role in investigating the global response of structures, especially in the framework of seismic risk  
52 analysis of existing structures and infrastructure. This study presents the optimal parameters  
53 characterization for the most-adopted steel constitutive models for smooth rebars using genetic  
54 algorithm (GA) and Bayesian updating. A refined finite element (FE) model implemented in the  
55 advanced open-source software OpeeSEES (McKenna et al., 2010) is adopted for simulating the  
56 actual response of steel reinforcement bars for different bar slenderness, i.e., the L/D ratios.  
57 Monotonic and cyclic tests from the literature of steel reinforcement bars are used for the calibration.  
58 Firstly, the numerical prediction of the inelastic buckling of ribbed rebars is conducted. The latter  
59 allows the validation of the effectiveness and accuracy of the adopted modelling approach by using  
60 the original formulation and default parameters of the examined steel constitutive models. Then, the  
61 FE model, along with the GA and Bayesian updating, is used to identify the optimal parameters for  
62 predicting the cyclic response of smooth steel rebars. Based upon the optimization procedure,  
63 regression analyses and probabilistic assessment of the examined parameters are performed. Three  
64 available constitutive steel models in OpenSEES (McKenna et al., 2010), namely Steel02 (Menegotto  
65 and Pinto, 1973; Filippou et al., 1983), SteelMPF (Menegotto and Pinto, 1973; Filippou et al., 1983;  
66 Kolozvari et al., 2015), and ReinforcingSteel (Kunnath et al., 2009), are investigated herein using the  
67 optimization procedure. The mechanical properties and the loading protocol for the smooth rebars are  
68 taken from Prota and Cosenza (2009). The key parameters of interest are the hardening ratio ( $b$ ), the  
69 initial curvature ( $R_0$ ) and the isotropic hardening in compression and tension ( $a1$  and  $a3$ ). The  
70 regression analyses and probabilistic assessment of the aforesaid model parameters are used as an  
71 effective way to facilitate the implementation of the stress-strain models of smooth rebars in advanced  
72 FE software for seismic risk analyses. The optimized variables are then utilized to validate the model  
73 further using available experimental monotonic compressive tests. Hence, a comprehensive  
74 parametric analysis is performed. The purpose of the parametric study is to develop an improvement  
75 of an existing analytical model -- initially developed by Prota and Cosenza (2006) -- for inelastic  
76 buckling of smooth rebars, which can be used either for robust seismic analyses or hand calculations  
77 for predicting the capacity of RC sections.

78

## 79 2. STATE-OF-ART OF NUMERICAL MODELS AND EXPERIMENTAL TESTS

80 A comprehensive literature review can be found for the effects of buckling on ribbed rebars, both  
81 experimental and numerical (e.g., Dhakal and Maekawa (2002); Bae et al., 2005; Kunnath et al.,  
82 2009; Massone and López, 2014; Akkaya et al., 2019, among others). Conversely, limited research  
83 has been conducted on the effects of inelastic buckling on smooth rebars (Cosenza and Prota, 2005;  
84 Prota et al., 2009). Dhakal and Maekawa (2002) conducted numerical investigations on the post-  
85 yielding buckling of reinforcing bars. Based on the numerical simulations, by using different L/D  
86 ratios, they provided a stress-strain model to account for the inelastic buckling for reinforcing bars.  
87 Then, the proposed method was combined with Menegotto-Pinto (1973) model for steel  
88 reinforcement to investigate the reliability of their numerical approach. The results showed an  
89 excellent agreement with the experimental test, both under monotonic and cycling loading.

90 **Bae et al. (2005)** carried out a large experimental campaign on 162 reinforcing bars tested under  
91 monotonic compressive loading. Results showed that L/D ratios greater than 6 demonstrated a  
92 negative instability once reached the onset of buckling; the increase in the initial geometrical  
93 imperfection resulted in reduced load-carrying capacity; L/D ratios smaller than four did not  
94 experience buckling even for large inelastic deformation. Furthermore, they provided a new  
95 relationship for the inelastic buckling of reinforcing steel, which was then validated against the  
96 experimental results showing a good agreement.

97 **Kashani et al. (2014)** carried out an experimental campaign on the effects of corrosion on ribbed  
98 rebars, which were then used as a model validation of the proposed buckling approach. A FE model,  
99 based on non-linear force-based elements was adopted. Results showed that the model could reliably  
100 predict the inelastic buckling response of corroded ribbed rebars under monotonic and cyclic  
101 loadings. The cyclic response of the reinforcing steel with different L/D ratios strongly depended  
102 upon the strain history, while high values of L/D reduced the onset of the critical load for the inelastic  
103 buckling (i.e., L/D = 15 and L/D = 20).

104 **Cosenza and Prota (2005)** carried out an experimental campaign on the compressive monotonic  
105 behaviour of “smooth rebars” to investigate the buckling effects using different values of the L/D  
106 ratio. For low L/D ratios (i.e., L/D = 5), the monotonic behaviour was almost coincident with the  
107 tensile tests. From L/D equal to 8, the plateau started decreasing with the increase of the L/D ratio.  
108 Finally, L/D greater than 20 showed a critical load close to or smaller than the yielding stress of the  
109 smooth reinforcing rebar. A modelling approach for simulating the inelastic buckling of smooth  
110 rebars as a function of the L/D ratio was provided. Such an experimental campaign was then extended  
111 for the cyclic response of smooth rebars in **Prota et al. (2009)**. They found that for values of L/D  
112 ranging between 5 and 7, the monotonic and tensile behaviour was not symmetric due to the  
113 progressive effects of buckling. Rebars started buckling earlier with the increase of the L/D ratio and  
114 approaching the yielding stress for values greater than 15. Moreover, the progressive effects of  
115 inelastic buckling appeared to increase the pinching especially for high values of the strain history. A  
116 critical review of the most used constitutive models for predicting the response of ribbed rebars was  
117 carried out. The comparison of those constitutive models showed that the non-linear expression  
118 (**Menegotto-Pinto, 1973; Monti-Nuti, 1982**) could sufficiently predict the behaviour of smooth rebars  
119 for L/D ratio lesser than 8 when inelastic buckling did not take place. However, for higher values of  
120 slenderness (L/D > 8) the formulation could not simulate the actual response of smooth rebars due to  
121 the change of curvature for each half cycle.

122 Although those few studies provided insights on constitutive models for simulating smooth rebars,  
123 there is a need to investigate such models by calibrating some of their parameters and using advance  
124 non-linear FE approaches. The post-elastic response of reinforcing steel depends on the strain history,  
125 so it is path-dependent (**Dhakal et al., 2002**). However, all previous studies on the cyclic response of  
126 smooth rebars referred to the experimental-analytical comparison and, therefore, this paper  
127 investigates the numerical-experimental comparison based on the only cyclic/monotonic tests known  
128 to the authors.

129 One of the most relevant methods used for structural optimization and design problems is the so-  
130 called Genetic Algorithm (GA). The pioneer of GAs **Holland (1975)** inspired many researchers to  
131 apply GA to many contexts and disciplines as a modern optimization technique. **Coello and**  
132 **Christiansen (2000)** applied the GA to enhance the design of two typical trusses based on multi-  
133 objective optimization. They proposed a new GA-based approach where the populations were

134 generated such that individuals represented only feasible solutions. The technique appeared to be  
135 faster and more accurate in optimizing the design of the two trusses. Perry et al. (2006) proposed a  
136 new modified GA strategy based on a space-reduction procedure to better identify the parameters of  
137 multiple-degree-of-freedom (MDOF) structural systems. They compared this approach to the  
138 standard GA, based on numerical simulations of 10-to-20 DOF shear-type structures, by considering  
139 structural parameters the mass, the damping and the stiffness. Results showed that the proposed  
140 method was able to reduce the average absolute error compared to the classical GA, improving the  
141 accuracy for the identification of structural parameters. Numerical modelling and experimental  
142 measurement are always affected by uncertainties (Celarek and Dolsek, 2013; Castaldo et al., 2019;  
143 Castaldo et al., 2020). As a result, it is paramount to account for modelling uncertainties. One possible  
144 solution to characterize these uncertainties is to adopt the Bayesian model updating. Such an approach  
145 is often adopted in structural engineering (Gardoni et al., 2002; Jalayer et al., 2010). Jalayer et al.  
146 (2010) adopted the Bayesian approach to quantify and update the model uncertainty parameters for  
147 the mechanical properties of materials and geometrical properties of construction detailing to assess  
148 the structural performance of existing RC structures based on the demand and capacity defined in the  
149 modern standard technical codes. A Bayesian framework was used in Gardoni et al. (2002) to  
150 construct probabilistic predictive capacity models for RC structural components.

### 152 3. RESEARCH SIGNIFICANCE

153 One of the most detrimental phenomena for existing substandard RC structures with smooth rebars  
154 and subjected to earthquake loadings is the inelastic buckling of longitudinal rebars. Such an inelastic  
155 instability may affect the global response of RC structures. As a result, it is essential to approach the  
156 inelastic buckling with advanced numerical analyses and machine learning algorithms to produce  
157 more reliable model parameters and, in turn, constitutive models to perform accurate seismic analysis  
158 and risk assessment. For this purpose, this study presents:

- 159 (1) An approach for optimizing the mechanical parameters to model smooth steel rebars under  
160 monotonic and cyclic loading. It employs genetic algorithms and Bayesian updating with the  
161 integration of a FE model of steel reinforcement. The latter is derived from an advanced open-source  
162 program platform for earthquake engineering applications;
- 163 (2) Insights on the relationships and probabilistic distributions for the model parameters of the most  
164 adopted constitutive models for steel reinforcements as a function of the bar slenderness. Such  
165 formulations are beneficial for engineering applications when employed in current stress-strain  
166 constitutive models to simulate the inelastic behaviour of smooth rebars;
- 167 (3) Improvement of an existing analytical model for inelastic buckling of smooth rebars based on the  
168 numerical and experimental results.

### 170 4. OPTIMIZATION PROCEDURE

#### 171 4.1 The Genetic Algorithm

172 A GA-based algorithm (Global Optimization Toolbox User's Guide, 2019) is used to calibrate  
173 conventional constitutive models for steel reinforcement to describe the inelastic buckling of smooth  
174 rebars. To investigate the load-bearing capacity and the seismic vulnerability of RC structures, civil  
175 engineers rely on FE approaches and the definition of parameters for existing constitutive models of  
176 concrete and steel reinforcement.

177 The most common approach for such optimization problems relies on the definition of an objective  
 178 function (e.g., the absolute error of the model and the empirical evidence) that may incorporate some  
 179 other constrained parameters to obtain a multi-objective optimization. This approach (Figure 1)  
 180 involves generating initial plausible populations of parameters chosen in pre-defined intervals derived  
 181 from the literature.

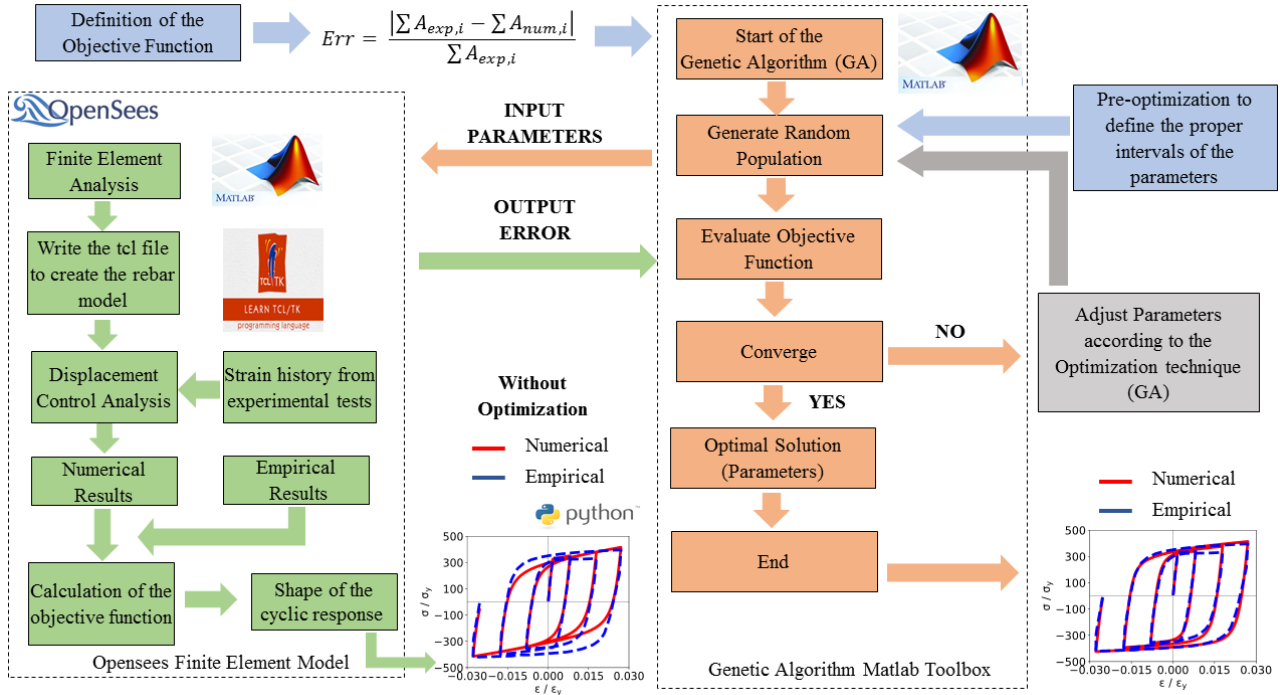


Figure 1. Flow-Chart of the optimization procedure

182  
 183  
 184

185 For instance, the constitutive models named Steel02 and SteelMPF are entirely defined by the  
 186 following parameters: yielding stress ( $f_y$ ), hardening ratio ( $b$ ), elastic modulus ( $E_s$ ), parameters  
 187 controlling the transition from the elastic to the plastic branch ( $R_0$ ,  $cR_1$ ,  $cR_2$ ) and the isotropic  
 188 hardening parameters ( $a_1$ ,  $a_2$ ,  $a_3$ ,  $a_4$ ). The yielding stress and the elastic modulus are kept constant  
 189 from the experimental results, as well as  $cR_1$ ,  $cR_2$  and  $a_2$ ,  $a_4$  are assumed equal to the default values.  
 190 Conversely,  $b$ ,  $R_0$ ,  $a_1$  and  $a_3$  are used to calibrate the numerical model with the experimental results.  
 191 Each of this generated population is then employed to construct a numerical (e.g., **OpenSEES**) model  
 192 of the smooth rebar under a cycling strain history. Then, the model is subjected to a load that is  
 193 consistent with the available experimental test in a sort of *virtual* laboratory test. The experimental  
 194 evidence and the numerical results from the model can then be used to calculate the error function.  
 195 In this study, the relative error between the hysteretic areas (Equation 1) of the test cycles is used.

$$Err = \frac{|\sum A_{exp,i} - \sum A_{num,i}|}{\sum A_{exp,i}} \quad (1)$$

196 The relative error defined in (1) targets the energy and it is the objective function to be minimized.  
 197 Once the analysis is completed and the error computed, the next generation parameters for the next  
 198 run will be adjusted according to the distance from the optimum. However, one of the main concerns  
 199 when applying GAs is the inherently random nature of all variables to be optimized. It is generally  
 200 necessary a pre-optimization process to reduce the variability of such parameters. The pre-  
 201 optimization is herein used to define proper intervals, depending on the slenderness ( $L/D$ ) ratio, by  
 202 running the numerical model with a small number of random populations. The last step allows

203 defining the intervals of the model parameters for the final optimization process with an assumed  
 204 variation per each variable (Figure 2). Once the variable intervals are defined, the GA performs the  
 205 analysis until the specified criteria are met.

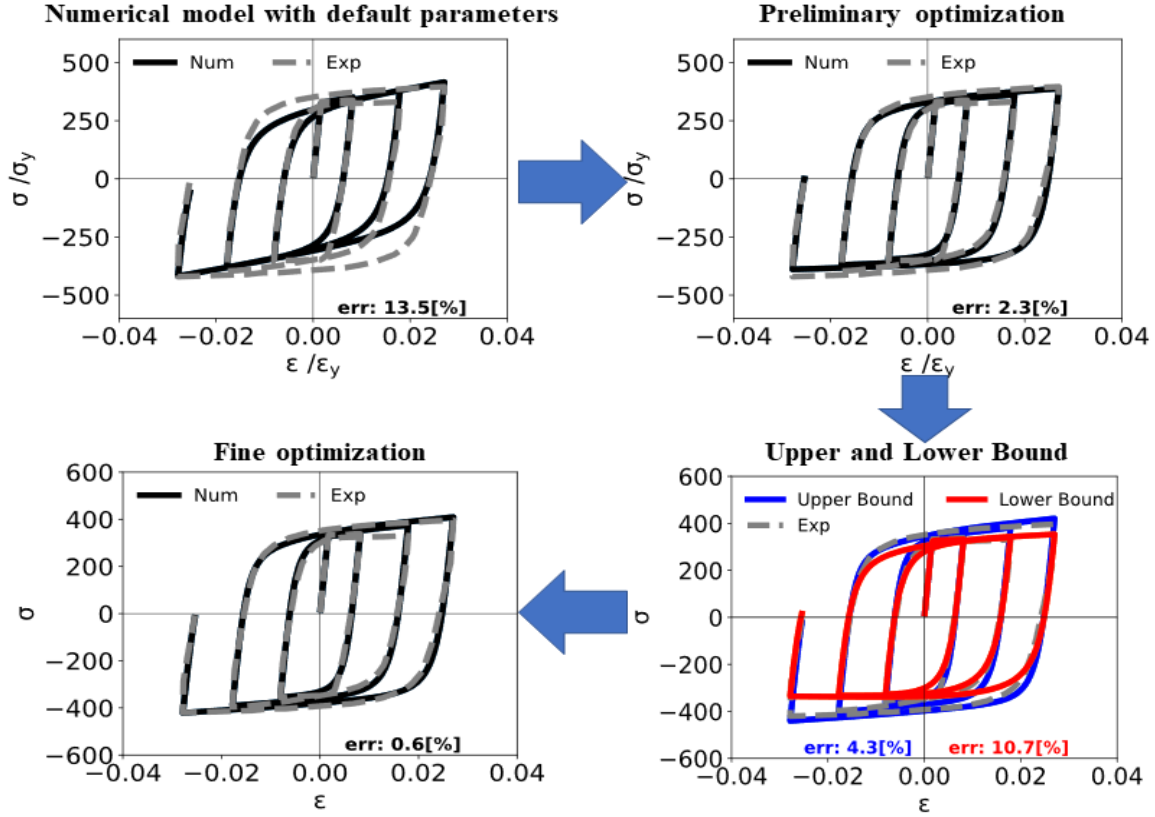


Figure 2. Genetic Algorithm Procedure

## 4.2 Bayesian Model Updating

210 Once the model parameters are estimated through the genetic algorithm, it is possible to characterize  
 211 the numerical modelling and the experimental measurement uncertainties. For this purpose, the  
 212 Bayesian updating is the recognized tool able to identify the probability for each model parameter  
 213  $P(\bar{\theta}|D_{exp.})$  (from the numerical model) given the experimental data ( $D_{exp.}$ ). The latter conditional  
 214 probability can be calculated as follows (e.g., Wasserman, 2013):

$$P(\bar{\theta}|D_{exp.}) = C^{-1}P(D_{exp.}|\bar{\theta})P(\bar{\theta}) \quad (2)$$

215  $\bar{\theta}$  is the vector containing the model parameters (i.e.  $R$ ,  $a1$ ,  $a3$  for Steel02 and SteelMPF, while  $R$  for  
 216 Reinforcing Steel),  $P(\bar{\theta})$  is the prior probability,  $P(D_{exp.}|\bar{\theta})$  is the likelihood, and  $C^{-1}$  is a  
 217 normalizing factor such that the area under the posterior curve is equal to 1. Based on the linear  
 218 regression analysis derived from the genetic algorithm for different rebar slenderness ( $L/D$ ) values, it  
 219 is possible to derive the prior probability  $P(\bar{\theta})$  for each model parameter. The likelihood is a  
 220 distribution representing the numerical modelling error compared to the experimental counterpart;  
 221 therefore, a standard normal distribution is adopted, with a mean equal to zero and an unknown  
 222 standard deviation added to the vector  $\bar{\theta}$ . The experimental data  $D_{exp.}$  can be either a single error term  
 223  $(\sum A_{exp} - \sum A_{num})$  for each test or a number of error terms for each cycle, assuming that the damage  
 224 of the rebar at each cycle is a function of only the previous cycle. In this second case, the likelihood  
 225 is the product of the standard normal pdf with unknown standard deviation calculated for each cyclic

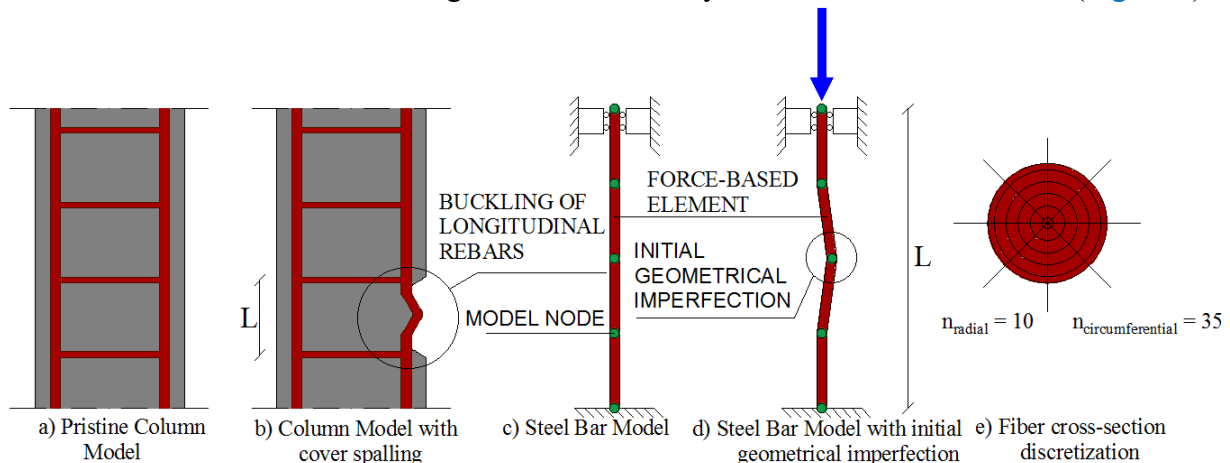
226 error. Equation 2 can be solved numerically. At the end of the analysis, the cumulative density  
 227 function of each marginal distribution is derived for each model parameter.

228

229 **5. FINITE ELEMENT MODEL OF THE STEEL BAR**

230 The non-linear behaviour of smooth rebars is modelled through spread plasticity beam-column force-  
 231 based elements (Spacone et al., 1996a and 1996b). Such an element, available in OpenSEES  
 232 (McKenna et al., 2010), neglects the effects of shear and bond-slip, but it can simulate the non-linear  
 233 behaviour of members under coupled bending moments and axial load. It is discretized in different  
 234 control points known as the integration scheme. Each integration point is characterized by fibre cross-  
 235 sections that define the non-linear behaviour of the element itself and where the stress-strain  
 236 relationship of each examined constitutive steel model is employed. The five points Gauss-Lobatto  
 237 integration scheme is herein used for computing the stress-strain at the section level. Since the aim is  
 238 to describe the buckling of steel bars, the linear transformation is not adequate to solve the large  
 239 inelastic displacement-small strain problems. Thus, this study uses the so-called co-rotational  
 240 formulation (Souza, 2000), which accounts for large displacements while remaining small  
 241 deformations along with the element.

242 To capture the inelastic buckling, an initial geometric imperfection is considered in the middle of the  
 243 element as to force an initial curvature, which turns into a linear transverse deviation of the element  
 244 to its longitudinal axis (Uriz et al., 2008). This imperfection is taken as  $L/1000$ , which is also the  
 245 maximum value stated by the ASTM A6/A6M (2019). As far as the boundary conditions are  
 246 concerned, one end is completely fixed (both translations and rotations); the other end is free to move  
 247 only along the longitudinal axis of the beam. Moreover, a fibre and element discretization schemes  
 248 were needed to obtain the best trade-off between accuracy and computational demand. From the  
 249 sensitivity analysis, the maximum number of elements equal to six is deemed acceptable to maintain  
 250 a realistic aspect ratio for the bar, as well as a circular cross-section with a number of radial fibres  
 251 equal to 10 and circumferential to 35 guarantees efficiency and small numerical effort (Figure 3).



252

253

254

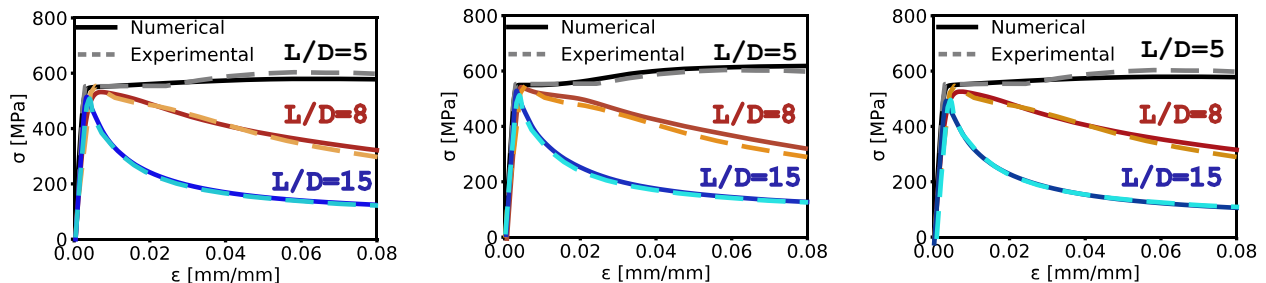
Figure 3. Buckling Model

255 A larger number of small elements will excessively reduce the bar length and results be no longer  
 256 realistic. Accurate preliminary tests were carried out and validated against experimental tests from  
 257 the literature (e.g., Kashani et al. 2014; Imperatore and Rinaldi, 2019). In this study, an adaptive  
 258 convergence algorithm was needed to perform a non-linear longitudinal displacement control analysis  
 259 (non-linear static analysis) for all the three examined constitutive steel models by using an initial

260 number of iterations equal to 100. The last observation comes after the convergence issues met for  
 261 the ReinforcingSteel material available in Opensees. If the convergence is not achieved, the number  
 262 of iterations is modified to 1000 while several solution algorithms are included to solve the non-linear  
 263 equations such as Newton, Krylov-Newton (Scott et al., 2010), ModifiedNewton and  
 264 NewtonLineSearch (Crisfield, 1991).

### 266 5.1 Model Validation for ribbed reinforcement bars

267 Earthquakes typically increase the compressive stresses that RC members are subjected to due to  
 268 frame effects and the potential vertical components (e.g., Di Sarno et al., 2011). Increasing  
 269 compressive stresses can induce instability of longitudinal rebars with a consequent significant lateral  
 270 displacement that may lead to inelastic buckling. Structural models should be able to capture the  
 271 inelastic buckling to obtain a more reliable and accurate local response of RC components. Typically,  
 272 buckling affects the post-yielding response of steel rebars which experience relevant softening  
 273 depending on the L/D slenderness ratio.



274 Figure 4. Experimental vs Numerical results. a) Steel02; b) ReinforcingSteel and c) SteelMPF.

277 Although this study focuses on the effects of the inelastic buckling on smooth rebars, it is essential to  
 278 validate the accuracy and the consistency of the numerical modelling approach against empirical  
 279 results of ribbed rebars reported in the literature, since the examined constitutive models were merely  
 280 calibrated for deformed bars. Despite this, the adopted FE approach can be eventually used for  
 281 parametric optimization of deformed rebars.

282 The comparison between the available experimental tests and the numerical approach reveals the  
 283 ability of the modelling approach to predict the post-yielding softening of steel reinforcement due to  
 284 buckling, even for small values of L/D, whereas its effects are negligible. Figure 4 show that the  
 285 proposed finite element approach is able to accurately predict the response of ribbed rebars under the  
 286 monotonic compressive loading for all constitutive steel models (used in this study) and different  
 287 values of L/D ratios. The results of the numerical simulations in Figure 4 are calculated using the  
 288 optimal discretization.

289 The validation of the current model for ribbed rebars under monotonic compressive loading and  
 290 affected by the buckling unveils that the modelling approach can be feasible for a parametric  
 291 optimization to predict the actual response of smooth rebars (Cosenza and Prota, 2009). However, a  
 292 study conducted by Carreno et al. (2020) shows that some parameters of the Menegotto-Pinto  
 293 constitutive model should be further investigated and optimized to identify the cyclic response of  
 294 ribbed rebars due to some discrepancies of the model in OpenSEES (McKenna et al., 2010) to  
 295 simulate the inelastic behaviour at each half cycle and the strain hardening after the yielding plateau.

296



## 6. CYCLIC RESPONSE OF SMOOTH REBARS UNDER INELASTIC BUCKLING

Very few studies have been conducted on the cyclic response of smooth rebars with different values of  $L/D$  ratios. Cosenza and Prota (2009) highlighted the main differences between the cyclic and monotonic response of smooth and ribbed bars based on an extensive experimental campaign. One of the main aspects referred to the dissipation of the hysteretic energy for both steel reinforcement. Subjected to the same strain history, the cyclic response curve of ribbed rebars was always internal to the previous ones compared to smooth rebars. The last observation is that smooth rebars showed minor stiffness damage (during unloading-loading) than ribbed rebars with a higher curvature for each cyclic response. Lesser curvature produced a much stronger Bauschinger effect for ribbed bars.

### 6.1 Steel02

Due to the optimal trade-off between simplicity and efficiency of the formulation, one of the most adopted constitutive models for non-linear steel reinforcement response is the model proposed by Menegotto and Pinto (1973), which refers to Steel02 in OpenSEES (McKenna et al., 2010). The stress ( $\sigma$ ) and strain ( $\varepsilon$ ) formulation is the following:

$$\sigma^* = b\varepsilon^* + \frac{(1-b)\varepsilon^*}{(1+\varepsilon^{*R})^{\frac{1}{R}}} \quad (3)$$

Equation (3) represents the curved transition from a straight-line asymptote (with slope equal to the initial stiffness) to another asymptote (with a slope corresponding to the hardening of the steel bar). The ratio between these two asymptotes is the hardening which refers to  $b$  in the eq. (3). The parameter  $R$  controls the shape of the transition curve (if  $R = \infty$  the curve becomes bi-linear) and allows the representation of the Bauschinger effect for each branch curve. The expression for  $R$  depends upon some parameters, such  $R_0$ , typically between 10 and 20,  $cR_1$  and  $cR_2$ , typically equal to 18.5 and 0.15, respectively, that are experimental parameters (e.g., Menegotto and Pinto, 1973; Filippou et al. 1983). Indeed, Filippou et al. (1983) proposed a refined modification of the original constitutive model for steel reinforcement. Since the isotropic hardening had relevant effects on the bars responsible for the crack closure of RC components under cyclic loading, they proposed a shift of the yielding asymptote position and, then, computing the new intersection point (unloading-loading) through a strain reversal rule. Hence, this shift rule suggested a new formulation with two other parameters  $a_3$  and  $a_4$ , which account for the isotropic hardening in compression and tension (default in Opensees  $a_3 = 0.00$  and  $a_4 = 1.00$ ). The last two parameters refer to  $a_1, a_2, a_3, a_4$  for Steel02 in Opensees. Further details can be found in Filippou et al. (1983). Using the FE approach and the default parameters, the comparison between experimental and numerical results (based on the average response of smooth rebars in Prota and Cosenza, (2006)) is carried out for different  $L/D$  ratios. Results in Figures 5 show that the use of the default parameters does not sufficiently allow the numerical model to simulate the response of a smooth rebar under cyclic loading, especially for low values of  $L/D$  ratio (i.e.,  $L/D = 5, 10$ ). Comparisons between the numerical approach and experimental tests, both in tension and compression, definitely seem to underestimate the energy dissipated for each half cycle. However, the last statement is not directly related to numerical approach, but rather the inability of the constitutive models, based on the provided mechanical properties, to capture the full hysteretic behaviour even when buckling ( $L/D < 5$ ) does not occur or at least is negligible. On the other hand, for higher values of  $L/D$  ratio, where inelastic buckling is most likely to occur, the model prediction overestimates the compressive and the tension behaviour of the steel bar anyhow.

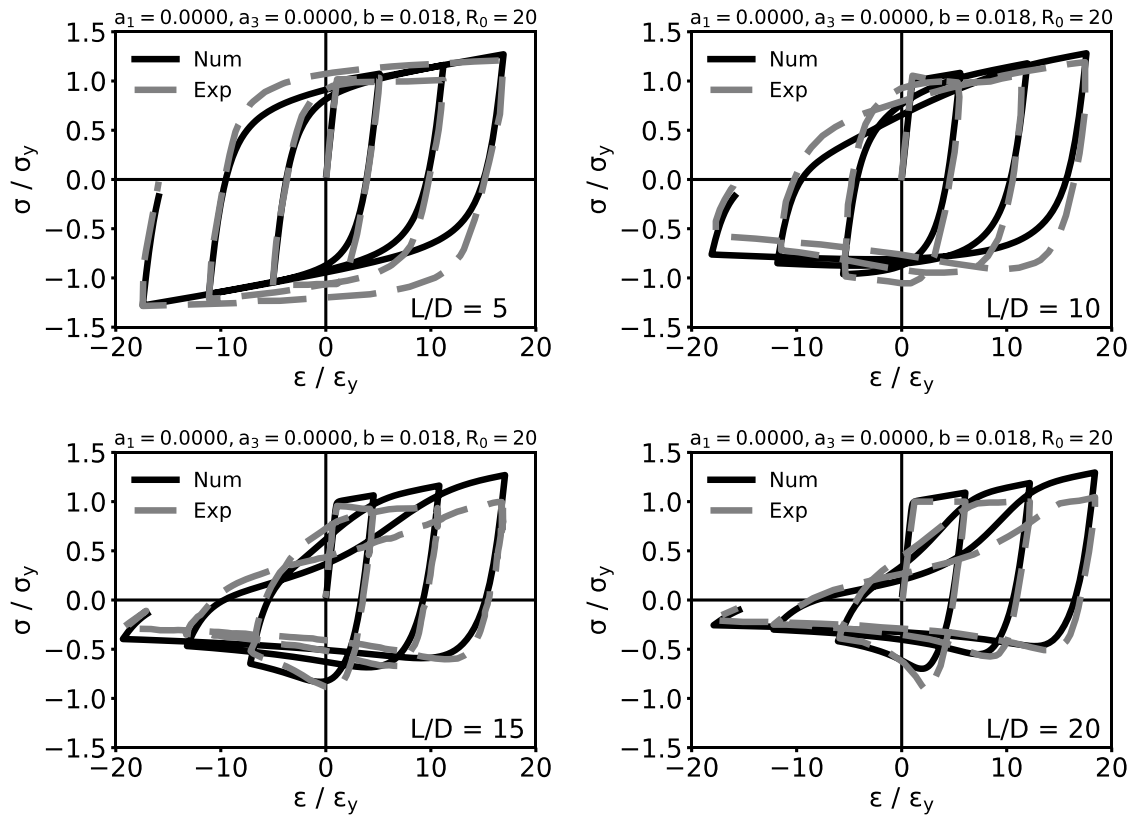


Figure 5. Numerical vs Experimental response of smooth bars with Steel02 in OpenSees

339  
340  
341

342 Moreover, the cyclic response does not seem conservative enough for the pinching effect, which is  
343 relevant for RC components under strong excitations.  $L/D$  ratios equal to 10 and 15 still appear to  
344 show significant discrepancies with the experimental results, mainly due to the small curvature and  
345 not calibrated isotropic parameters assigned to the constitutive models. On the other hand, when the  
346 curvature and the isotropic parameters approach the ideal values (i.e.,  $L/D = 20$ ), based on the  
347 optimization procedure, the model starts efficiently predicting the cyclic response of smooth rebars.  
348 The above discussion suggests a need for a parametric optimization of the main parameters of such  
349 constitutive model, especially for existing RC infrastructures and buildings under strong earthquakes.  
350 The parameters to be optimized are chosen based on the observed experimental data, such as:

- 351 -  $R_0$ , the curvature is higher for smooth rebars and appears to change for different slenderness  
352 ratio;
- 353 -  $b$ , the hardening ratio; according to the experimental tests, the energy dissipated by smooth  
354 bars is certainly higher than ribbed bars; thus, an appropriate estimate of the hardening  
355 asymptote is of reasonable importance;
- 356 -  $a_1, a_3$ , the compressive and tension isotropic parameter; these two parameters allow to capture  
357 the higher energy dissipation for each half cycle.

358 Conversely, some parameters, such as  $a_2, a_4$  and  $cR1$  and  $cR2$ , are kept fixed as in the original  
359 formulation, since their change will turn into a complete shift of the curve shape.

360 The outcomes of the optimization procedure are given in [Figure 6](#).

361 Results from simulations notably illustrate that the proposed procedure can accurately and adequately  
362 predict the response behaviour of smooth rebars under a cyclic strain loading. The hysteretic energy  
363 dissipation of each half-cycle, a crucial measure of a component under cyclic loading, is well-  
364 predicted, thus, allowing an adequate response if such stress-strain curves are employed in the fibre-

365 section of RC components. Moreover, the bar-buckling affects the strength capacity and the hysteretic  
 366 energy dissipation with the increase of the slenderness ratio  $L/D$ .  
 367

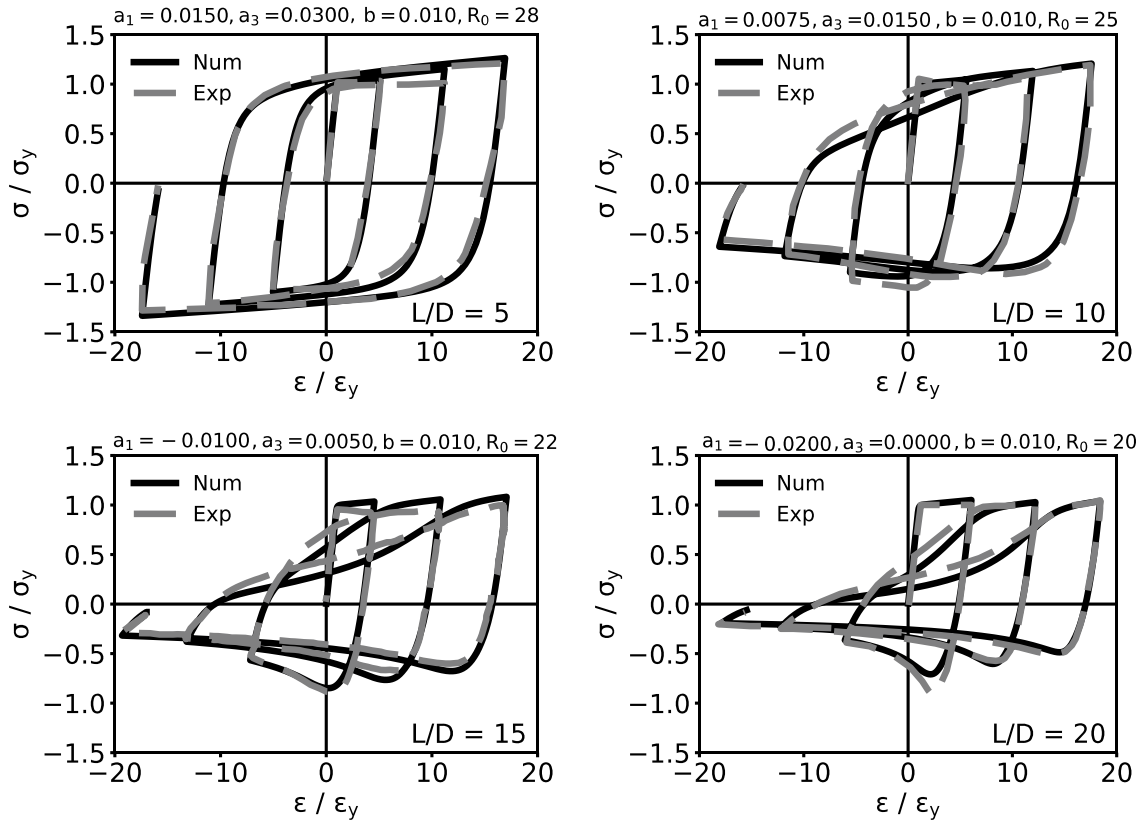


Figure 6. Numerical vs Experimental with optimized parameters

368  
 369  
 370  
 371 Observations from the optimization procedure show that the value of the hardening ratio appears to  
 372 be constant regardless of the increase of the slenderness. Particularly, its value is reduced by a factor  
 373 of 1.8 compared to the initial hardening ratio provided in **Cosenza and Prota (2008)**.  $R_0$ , which denotes  
 374 the value of  $R$  during the first loading, ranges between 28 and 20 with the increase of the slenderness,  
 375 demonstrating almost a linear variation with  $L/D$ . The last consideration highlights the increasing  
 376 effects of the bar-buckling on the initial curvature of the constitutive model. Furthermore, it is worth  
 377 noting that the increasing value of the slenderness ratio  $L/D$  denotes a significant effect on the  
 378 buckling initiation, which is most likely to occur at lower strain for the same steel bar (but with  
 379 different  $L/D$ ). As a result, the post-yielding branch is characterized by an exponential reduction of  
 380 the strength capacity with a change of the curvature (negative), especially for high values of  $L/D$   
 381 ratios, as can be seen in **Figures 6c and 6d**. Regression analysis is then carried out to accurately  
 382 describe the correlation of the optimized parameters to the slenderness ratio.

383 **Figures 7** show that the linear interpolation seems to be an appropriate estimation of the optimized  
 384 parameters to define the inelastic cyclic response of smooth rebars. The improved parameters can  
 385 then be employed to define the stress-strain steel model for the cross-section fibres to obtain a more  
 386 accurate response of RC components.

387 **Figures 8** shows the numerical simulations from the Bayesian model updating. The marginal  
 388 distributions of the model parameters ( $R_0, a_1, a_3$ , in this case) are accurately fitted using normal  
 389 distributions. However, it should be stressed that the standard deviations are equal to those obtained  
 390 from the GA application. The last observation comes from the likelihood function, which is defined

391 by only one data (the total error of the full hysteretic curve). Instead, having more data some  
 392 differences between posterior and prior may arise.  
 393

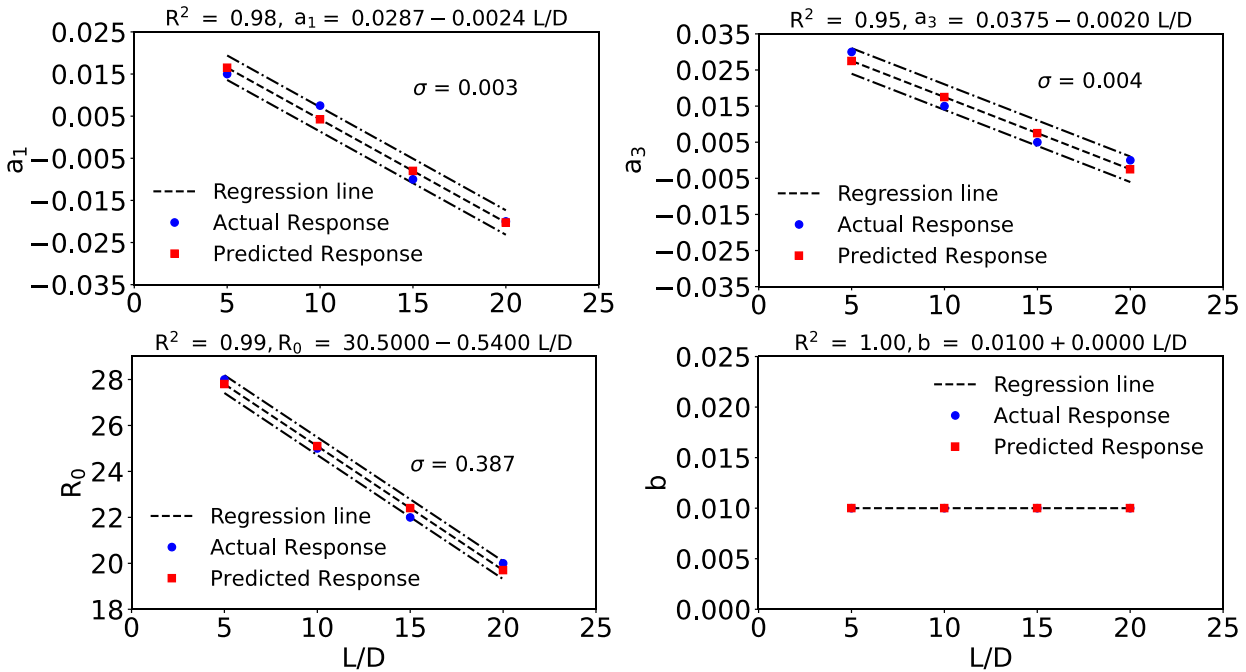


Figure 7. Regression Analysis of the optimized parameters

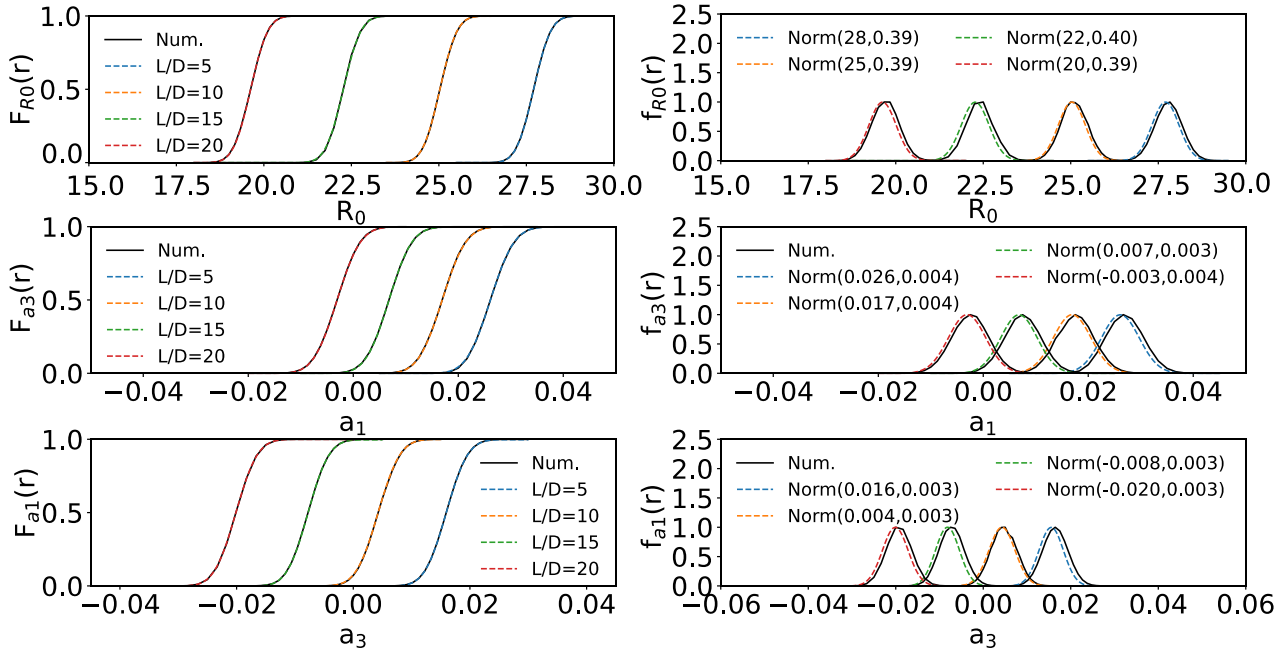
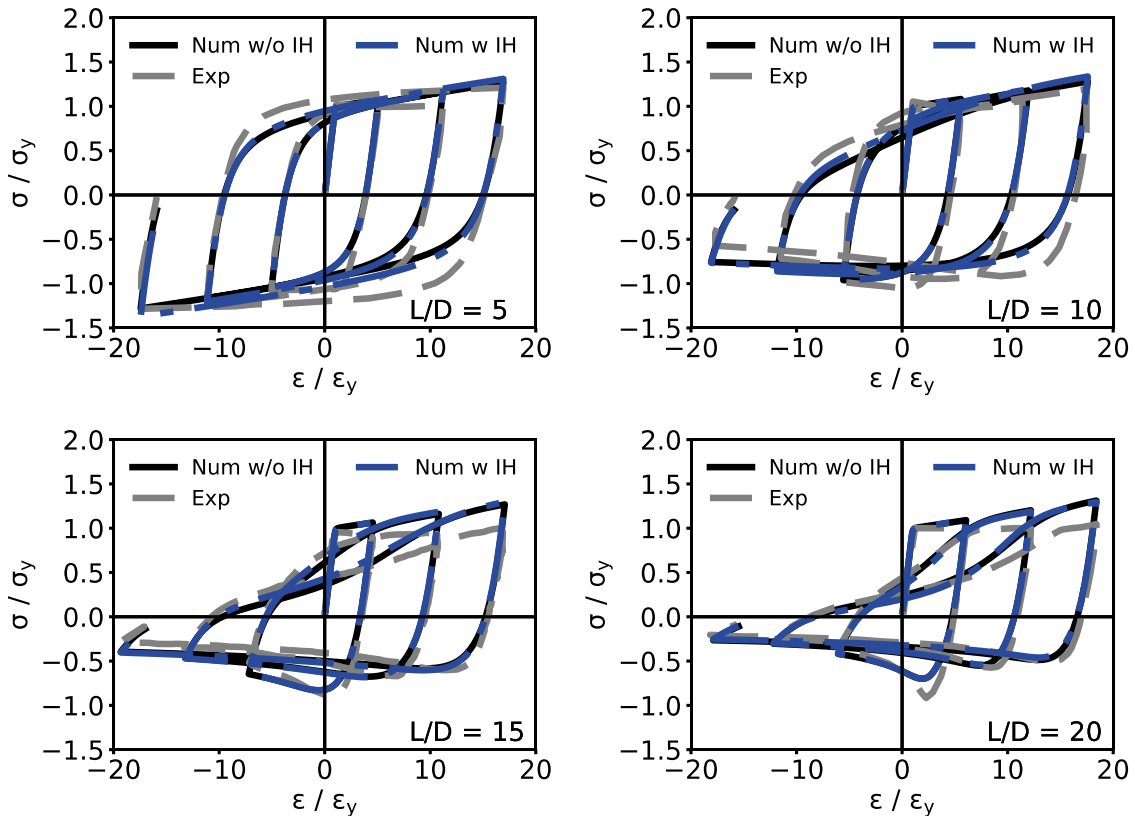


Figure 8. Bayesian model Updating of the model parameters for different  $L/D$  ratio

## 6.2 SteelMPF

400 **Kolozvari et al. (2015)** implemented a new material named SteelMPF, which accounts for several  
 401 new characteristics compared to the existing Steel02. The SteelMPF constitutive model allows  
 402 defining the yield stress and the hardening ratio in both tension and compression, as well as the pre-  
 403 yielding cyclic curvature degradation ( $R$ ) for loading-unloading. Furthermore, they have addressed  
 404 and solved the overshooting issue of the original formulation in Steel02 when subjected to partial  
 405 dynamic unloading. The partial unloading developed no longer feasible hardening behaviour of the

406 model itself and, as a result, it could have caused an inappropriate estimation of the seismic capacity  
 407 of RC components. The authors remind the original work of **Kolozvari et al. (2015)** for further details.  
 408 The current model (e.g., SteelMPF) was still calibrated for ribbed rebars and some default values are  
 409 available for its use when defining the stress-strain in the fibre-section of RC components. Thus, a  
 410 comparison between experimental and numerical results via the proposed FE model is needed to  
 411 investigate if such default parameters are suitable for simulating the cyclic response of smooth rebars.  
 412 There are two kinds of default parameters, which can be found in **Filippou et al. (1983)** and **Kolozvari**  
 413 **et al. (2015)**, to reproduce the response of ribbed steel reinforcement: a) the first one does not account  
 414 for the isotropic hardening, both in compression and tension, so the default parameters are  $a_1 = a_3 =$   
 415  $0.00$  and  $a_2 = a_4 = 1.0$ ; b) the second one yields the isotropic hardening, both in tension and in  
 416 compression, and the default parameters are  $a_1 = a_3 = 0.01$  and  $a_2 = a_4 = 7.0$ .  
 417 To find out if such suggested default values are suitable, both cases, previously mentioned, are herein  
 418 analyzed and compared to experimental results from the literature.  
 419 **Figures 9** show that the FE model does not correctly reproduce the inelastic response of smooth rebars  
 420 when employing default parameters. One of the main reasons for such inconsistency with the  
 421 experimental outcomes lies in the difference between the constitutive model of the two types of steel  
 422 reinforcement. For low values of slenderness (e.g.  $L/D = 5$  and  $10$ ), the discrepancy with the  
 423 experimental results derives mostly from the dissipated hysteretic energy, which is underestimated  
 424 for large values of the strain loading. Conversely, the FE approach seems to overvalue the mean  
 425 compression stress at large strains. When the slenderness ratio ( $L/D > 15$ ) approach higher values,  
 426 whereas the default parameters almost coincide with the optimized ones, the numerical model appears  
 427 to match the experimental results. However, the mean tension stresses are still higher than the  
 428 experimental results.



429  
 430 *Figure 9. Numerical vs Experimental response of smooth bars with SteelMPF in Opensees. (Keynote: IH – Isotropic*  
 431 *Hardening)*

432

433 Nevertheless, SteelMPF allows the definition of yield stress ( $f_y$ ) and hardening ratio ( $b$ ) both for  
 434 compression and tension, it was chosen to keep both values as one variable to simplify and not  
 435 overwhelm the optimization procedure. The variables for the optimization process are the following:  
 436 the isotropic hardening in compression and tension ( $a_1, a_3$ ), hardening ratio ( $b$ ) and the initial value  
 437 of the curved transition ( $R_0$ ). The results are given in Figure 10.

438 Figures 10 demonstrate that the joint approach effectively captures the inelastic behaviour of smooth  
 439 rebars under cyclic loading and different  $L/D$  ratios. The compressive and tensile behaviours are  
 440 accurately reproduced by the FE model of the smooth bar in OpenSEES (McKenna et al., 2010) by  
 441 optimizing some of the previously mentioned parameters needed to define the constitutive model.  
 442 The error in the hysteretic energy dissipation is very small for each half cycle, while significant  
 443 improvement can be seen in the compressive response compared to the existing model Steel02  
 444 (Figures 6). It is worth noticing a slight overestimation of the tension stresses for high values of the  
 445 strain loading. However, this minor variation does not negatively affect the global response of the  
 446 numerical approach to the experimental results. Indeed, the proposed approach is successfully able to  
 447 predict the pinching response of the material, which is a relevant aspect for RC components under  
 448 strong excitations.

449 A value of slenderness  $L/D$  equal to 20 indicates that the numerical approach undervalues the  
 450 compressive peak stress. However, this is not directly related to the FE model itself but rather to the  
 451 randomness of the experimental campaign. The experimental compressive stress of  $L/D = 20$  is  
 452 greater than the corresponding value for  $L/D = 15$ . Apart from this observation, the optimization  
 453 procedure and the proposed FE model can capture the full inelastic response even when longitudinal  
 454 bars are subjected to strong buckling effects.

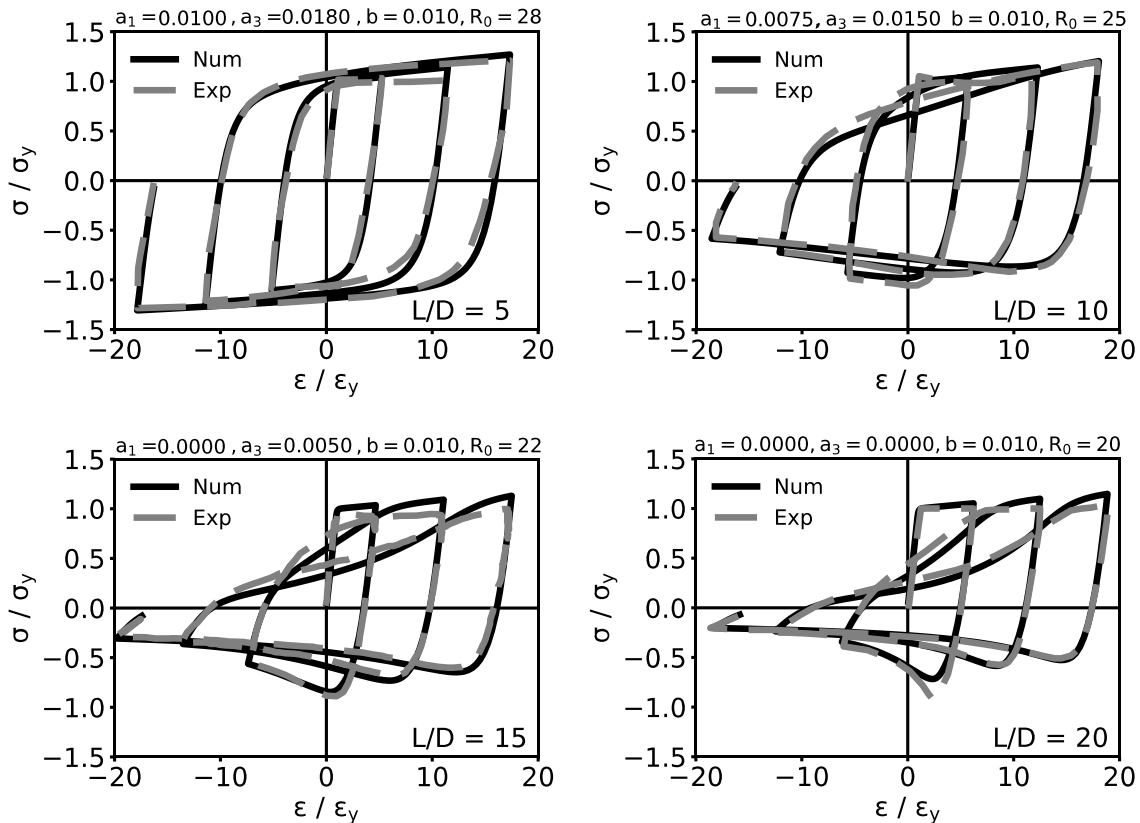


Figure 10. Numerical vs Experimental with optimized parameters

455

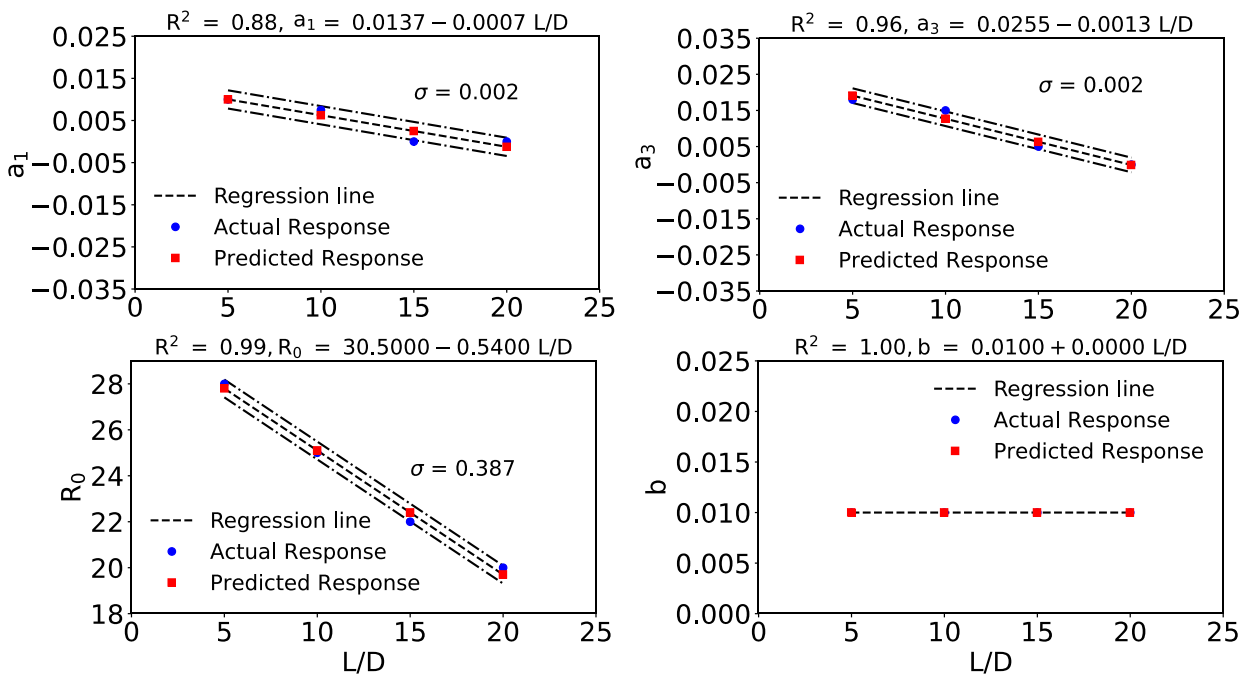
456

457

458 Figures 10 indicate that the increasing value of the slenderness ratio, corresponding more stirrups  
 459 spacing, significantly affects the dissipation energy of smooth steel reinforcement. The onset of  
 460 instability reduces the hysteretic energy dissipated at each half cycle, and the strength capacity and  
 461 stiffness, especially while unloading from the compressive side. The model is also able to reliably  
 462 predict the change of the curvature with the increase of the  $L/D$  ratio as can be seen for  $L/D = 15$  and  
 463  $L/D = 20$ .

464 A regression analysis (Figures 11) is then carried out to investigate any correlation between the  
 465 optimized parameters and slenderness ratios. Such correlations aim to facilitate users to simulate the  
 466 cyclic behaviour of smooth rebars when using the SteelMPF model to assess the inelastic capacity of  
 467 RC structures.

468 The linear interpolation in Figures 11 appears to be a proper estimation of the actual response from  
 469 the numerical simulations. The hardening ratio has not any variation but reduced by a factor of 1.8  
 470 compared to the original value as for Steel02. The initial curvature  $R_0$  decreases with the increase of  
 471 the slenderness ratio, and the values of the isotropic hardening start decreasing with the growing  
 472 instability of longitudinal rebars. The linear relationships are quite close to the ones provided for  
 473 Steel02, mainly due to the modification brought to the SteelMPF model and it has produced better  
 474 results in the inelastic response of smooth bars.



475  
 476 Figure 11. Regression Analysis of the optimized parameters  
 477

478 The numerical simulations from the model updating approach are shown in Figures 12. The marginal  
 479 probability of each model parameter ( $R_0$ ,  $a_1$ ,  $a_3$ , in this case) can be adequately fitted through normal  
 480 distribution with mean and standard deviation almost coincident with the outcomes from the GA.

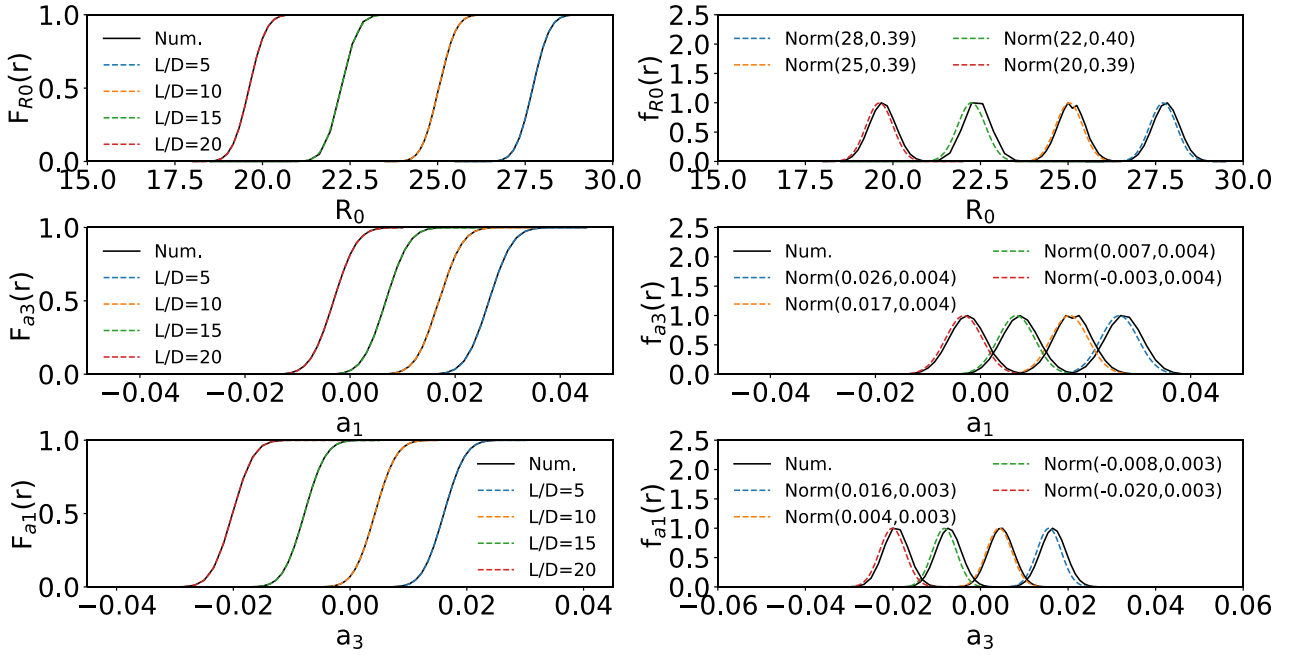


Figure 12. Bayesian Model Updating of the model parameters for different L/D ratio

### 6.3 ISOTROPIC HARDENING PARAMETERS

Figures 7 and 11 show that the regression analysis for the isotropic parameters ( $a_1, a_3$ ), based on the numerical optimization results for STEEL02 and STEELMPF, leads to negative values with the increase of the bar slenderness ratio. It is then recalled that the formulations characterizing the isotropic hardening in tension and compression are as follows:

$$f_{st} = f_y \frac{a_3}{a_4^{0.8}} \left[ \frac{\varepsilon_p^{MAX} - \varepsilon_p^{MIN}}{2\varepsilon_y} \right]^{0.8} \quad (4a)$$

$$f_{st} = f_y \frac{a_1}{a_2^{0.8}} \left[ \frac{\varepsilon_p^{MAX} - \varepsilon_p^{MIN}}{2\varepsilon_y} \right]^{0.8} \quad (4b)$$

where  $\varepsilon_p^{MAX}$  and  $\varepsilon_p^{MIN}$  are the minimum and the maximum strain recorded at the latest strain reversal.

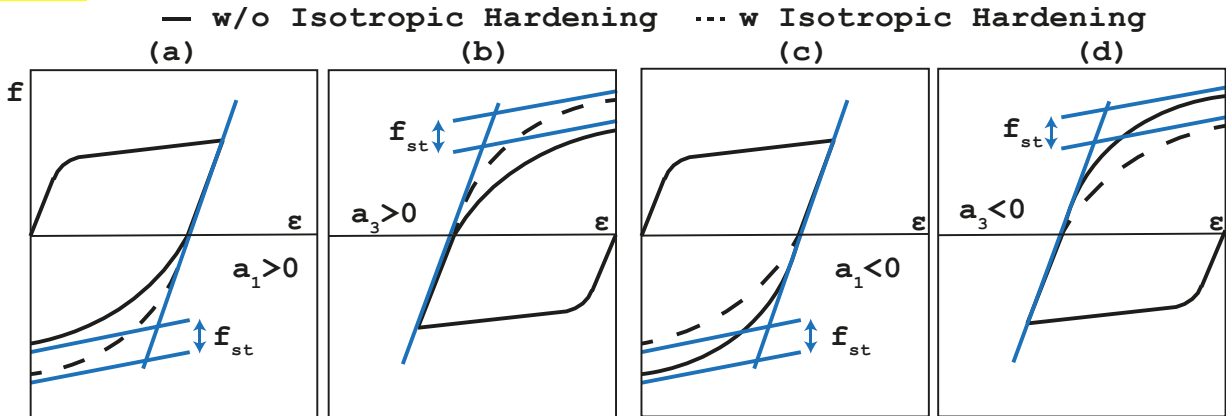


Figure 13. Stress shift of the Hardening Asymptote: (a) and (c) Compression ( $a_1 > 0$  and  $a_1 < 0$ ); (b) and (d) Tension ( $a_3 > 0$  and  $a_3 < 0$ )



496 Such formulations illustrate that without strong buckling effects (e.g.,  $L/D < 8$ ), the post-yielding  
 497 stress shift ( $f_{st}$ ) moves in the positive direction, which implies that each branch curve is external to  
 498 the previous one reaching out the last reversal strain at higher stresses (positive shift). On the other  
 499 hand, when the steel rebars are subjected to significant inelastic buckling effects, the post-yielding  
 500 asymptote tends to be negative and moving downward (Figure 13a and 13b); thus, the following  
 501 cyclic curve reaches the latest strain point at lower values of the stress (negative shift, Figure 13c and  
 502 13d). These observations indicate the physical meaning behind the negative values of the isotropic  
 503 parameters for high values of the slenderness ratio ( $L/D > 8$ ).

504

#### 505 6.4 Reinforcing Steel

506 One of the possible constitutive models available in OpenSEES (McKenna et al., 2010) for simulating  
 507 the response of steel reinforcement in RC cross-sections is the “ReinforcingSteel” material. This  
 508 model was introduced in Kunnath et al. (2009) and then implemented in the open-source platform  
 509 Opensees. It includes many features that the previous-examined models (e.g., Steel02 and SteelMPF)  
 510 do not incorporate, such as buckling and low-cycle fatigue.

511 The material refers to the original formulation of Chang and Mander (1994) as their monotonic  
 512 compressive and tensile stress-strain curves are used as boundary limits, while two different  
 513 formulations are employed to predict the effects of inelastic buckling (Gomes and Appleton, 1997;  
 514 Dhakal and Maekawa, 2002). The low-cycle fatigue, instead, is considered through the formulation  
 515 of Coffins-Manson (1971).

516 The monotonic and cyclic behaviour of the proposed uniaxial material was validated against a set of  
 517 experimental campaigns reported in the literature. Results from numerical simulation showed that the  
 518 model was able to capture with good accuracy the response of ribbed rebars.

519 On the other hand, the constitutive material demonstrated some discrepancies when using the  
 520 buckling formulation. The results showed that the uniaxial material underpredicted the compressive  
 521 behaviour of ribbed rebars, mainly due to the independence of the buckling model from the bar  
 522 diameter, which eventually affects the global compressive response. For many other details, the  
 523 authors remind the original study of Kunnath et al. (2009).

524 Since this study investigates the inelastic buckling of smooth rebars, the definition of the  
 525 ReinforcingSteel material here only refers to the mechanical properties of steel bars without including  
 526 the buckling and low-cyclic fatigue models.

527 The uniaxial material in OpenSEES (McKenna et al., 2010) is completely defined by the following  
 528 mechanical properties: yielding and ultimate stress, strain corresponding to the initial hardening,  
 529 tangent at the initial hardening (which includes the hardening parameter  $b$ ), the strain at the peak  
 530 stress, and Menegotto-Pinto parameters (which refers to  $R_0$ ).

531 Figure 14 shows that the FE approach is not sufficiently adequate for predicting the cyclic behaviour  
 532 of smooth rebars for different slenderness ratio. The numerical simulations demonstrate that the  
 533 original formulation is not too far beyond the experimental results except for  $L/D$  greater than 10  
 534 where a slight underestimation for the compressive behaviour can be observed. Hence, based on those  
 535 comparisons, the optimization parameters are the hardening ratio ( $b$ ) and the value  $R_0$  of the initial  
 536 curvature.

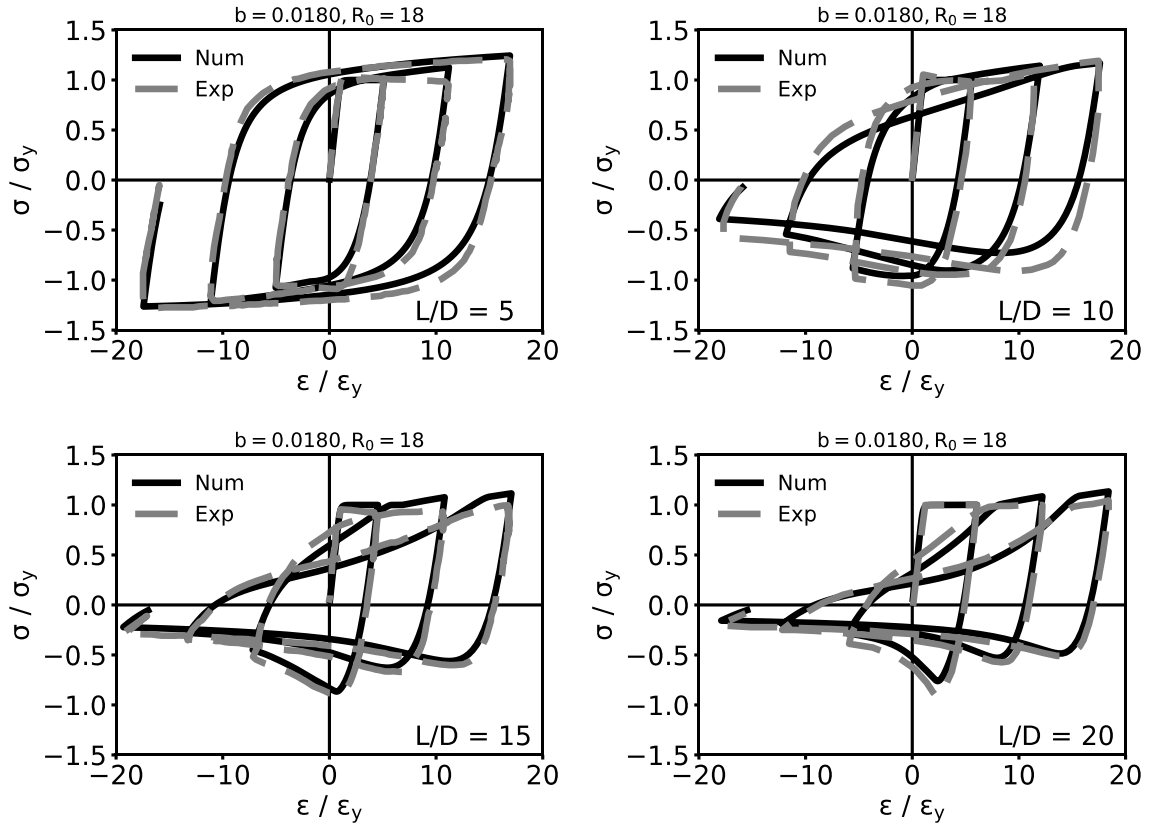


Figure 14. Numerical vs Experimental response of smooth bars with SteelMPF in Opensees

537  
538  
539

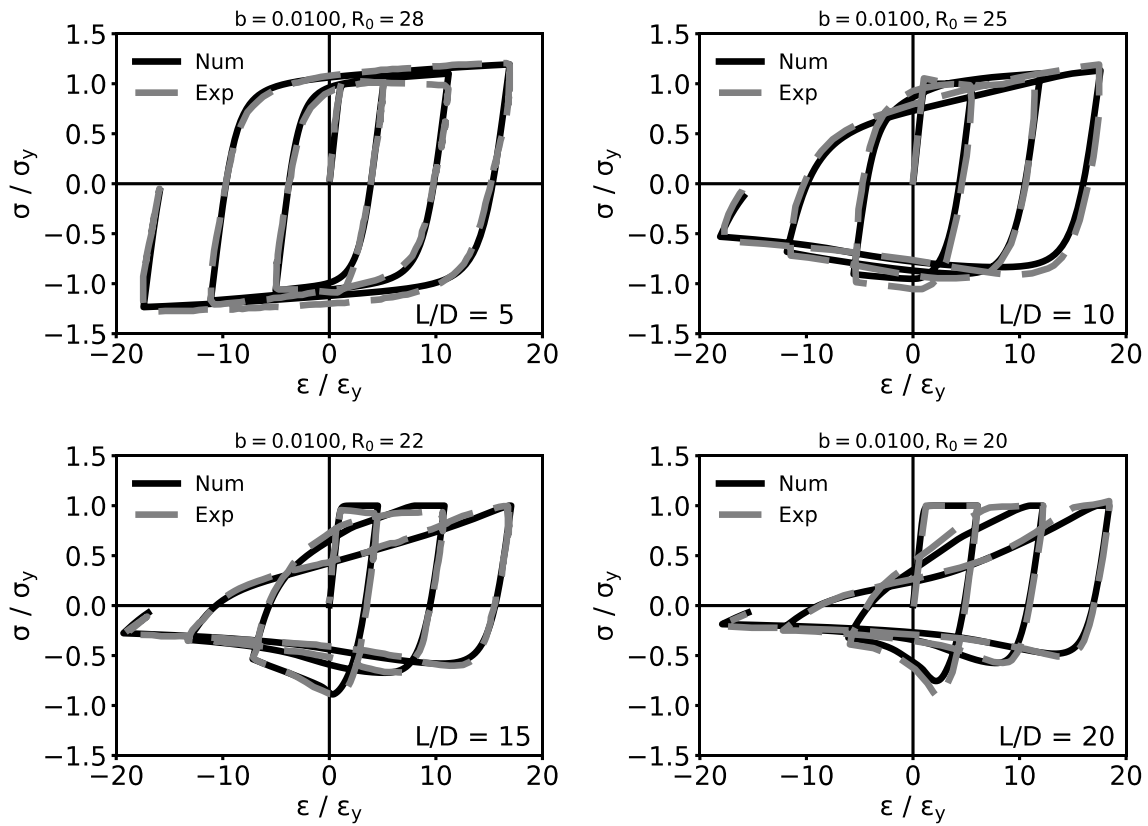


Figure 15. Numerical vs Experimental with optimized parameters

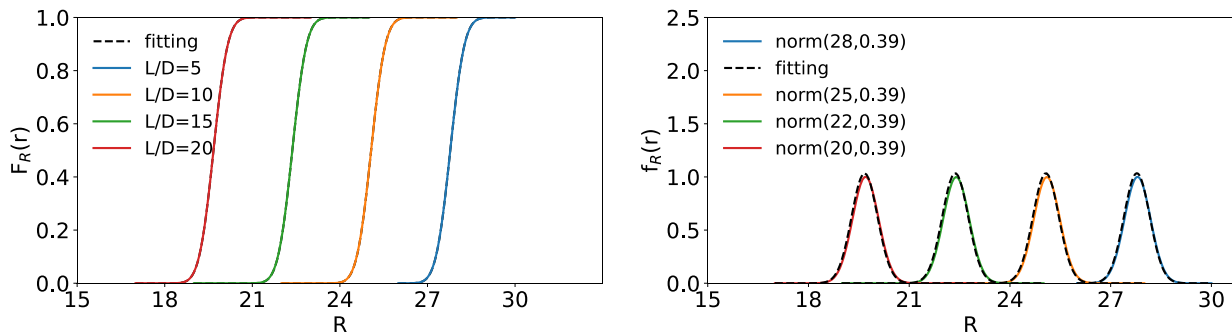
540  
541  
542

543 **Figures 15** illustrates that the proposed modelling approach can accurately simulate the inelastic  
 544 response of smooth rebars. Compared to the other two examined uniaxial materials (e.g., Steel02 and  
 545 SteelMPF), there is an additional improvement at each half cycle of the numerical response.  
 546 Moreover, the FE model can predict the peak both in tension and compression with excellent  
 547 accuracy.

548 The curvature inflection, especially for high values of  $L/D$ , and the pinching effects, are effectively  
 549 reproduced by the numerical simulations. The minor overestimation of the tensile stresses seen for  
 550 the previously examined uniaxial materials completely disappears as the model can easily follow up  
 551 the tensile behaviour recorded in the experimental tests. The optimized parameter  $R_0$  decreases with  
 552 the increase of the slenderness ratio, while the hardening ( $b$ ) remains constant but reduced by a factor  
 553 equal to 1.8 compared to the original value.

554 Finally, there is no need for a regression analysis as the results for the initial curvature and hardening  
 555 ratio have the same trend seen in **Figures 7c-7d** and **Figures 10c-10d**.

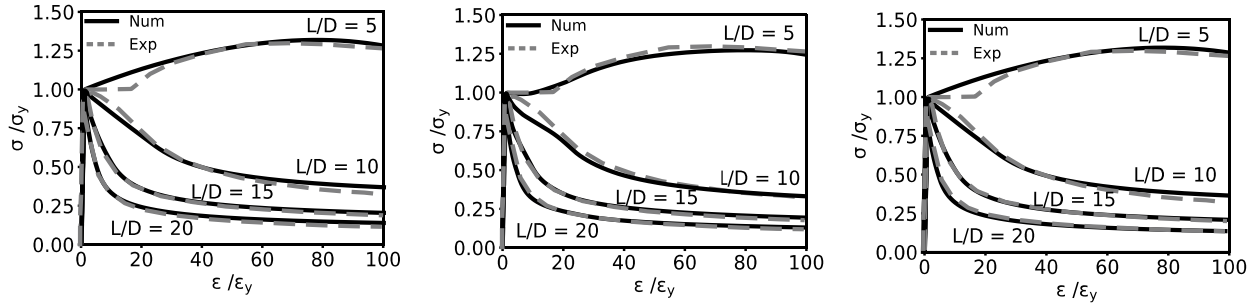
556 Using the linear regression to define the prior as defined in section 4.3, the model updating is applied  
 557 to account for the uncertainties concerning the numerical modelling and the experimental results.  
 558 Since the hardening ratio values are constant, the only parameter to be used in the Bayesian approach  
 559 is the initial curvature  $R_0$ . **Figure 16** shows the results of the numerical simulations. The marginal  
 560 distributions of the model parameter for different values of  $L/D$  are well fitted by a normal distribution  
 561 with a mean whose values also verify the accuracy of the genetic algorithm. In this case, as in the  
 562 likelihood function, only one data is used; the posterior and the prior are identical. Having more data  
 563 differences may arise. The distributions obtained herein can be used as prior if newly available data  
 564 will be available.



565  
 566 **Figure 16.** Probabilistic distribution of the model parameters based on the model updating  
 567

### 568 **6.5 Monotonic inelastic Buckling**

569 Using the FE modelling approach of the steel bar, the optimized parameters from the regression  
 570 analysis and the strain history from experimental results, the monotonic axial compression response  
 571 of smooth steel reinforcement is here investigated. The non-linear static analysis (in displacement  
 572 control) is conducted without involving strain reversal rules as suggested in **Mau et al. (1989)**, but  
 573 rather an increasing compressive loading is applied until failure. The outcomes from the numerical  
 574 simulation are shown in **Figure 17a, 17b** and **17c**.



575

576

Figure 17. Monotonic numerical vs experimental results. (a) Steel02, (b) ReinforcingSteel and (c) SteelMPF

577

578

The latter figure demonstrates that the proposed approach and model parameters can efficiently predict the average compressive stress-strain response of longitudinal smooth bars under severe inelastic instability. Steel02 (Figure 17a) and SteelMPF (Figure 17b) show similar results since they follow the same original formulation (Menegotto-Pinto, 1973 and extended by Filippou et al., 1983). However, the last constitutive models are not able to predict the yielding plateau, but this observation is more related to the concept of material formulation and implementation. Despite this drawback, the model can accurately simulate the overall monotonic compressive behaviour with a slight not conservative response for  $L/D$  equal to 10. Similarly, the ReinforcingSteel (Figure 17c) material can capture the empirical results and, indeed, adequately simulate the yielding plateau for low slenderness ratio values (e.g.,  $L/D = 5$ ). The model seems only to slightly underpredict the monotonic response for an  $L/D$  ratio equal to 10, but this could lie into the uncertainty of the experimental campaign and observed data.

590

## 591 7. ANALYTICAL MODEL OF INELASTIC BUCKLING

592

Based on an accurate assessment of the stress-strain curves from numerical simulation, all the constitutive models exhibit a compressive behaviour that can be ideally divided into three different stages:

595

(a) Linear elastic, the stress increases until the yielding of the steel reinforcement without being affected by instability (typically for  $L/D$  lower than 20, after that the onset of buckling starts for values lower than the yielding stress);

598

(b) Stress follows the path of the tensile behaviour of smooth reinforcements until reaching the onset of buckling;

600

(c) After the onset of buckling, there is an increasing non-linear softening (exponential decrease) that depends on the slenderness ratio  $L/D$ .

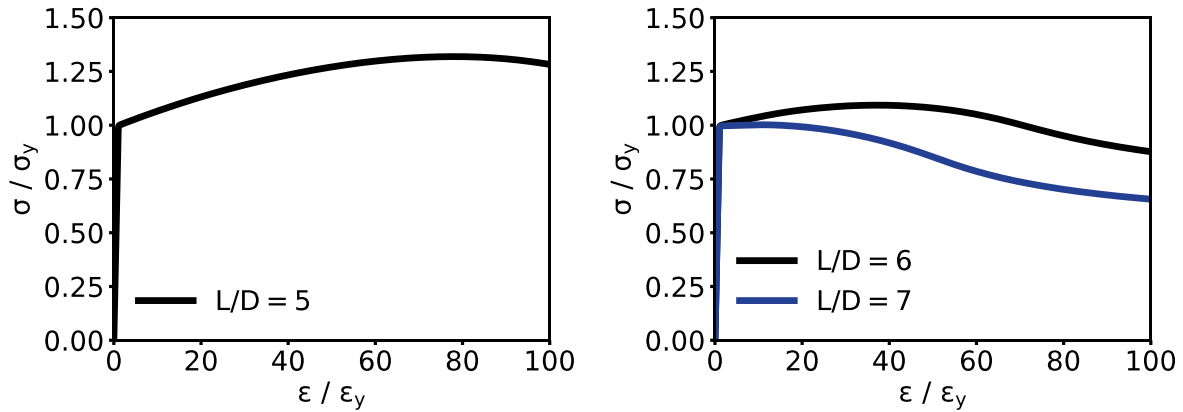
602

Numerical methods, based on advanced FE approaches, are not always straightforward to use, so analytical models are simple and effective ways to support civil engineers for performing non-linear fibre-based analyses of RC structures including the effects of inelastic buckling. When the optimization mechanisms are understood and the numerical behaviour aligns with the physical expectations, analytical models can be derived using the numerical tool extensively at a minimal cost. As a result, a numerical parametric study is conducted to investigate the effect of inelastic instability on the yielding plateau and post-buckling softening for different slenderness ratios.

609

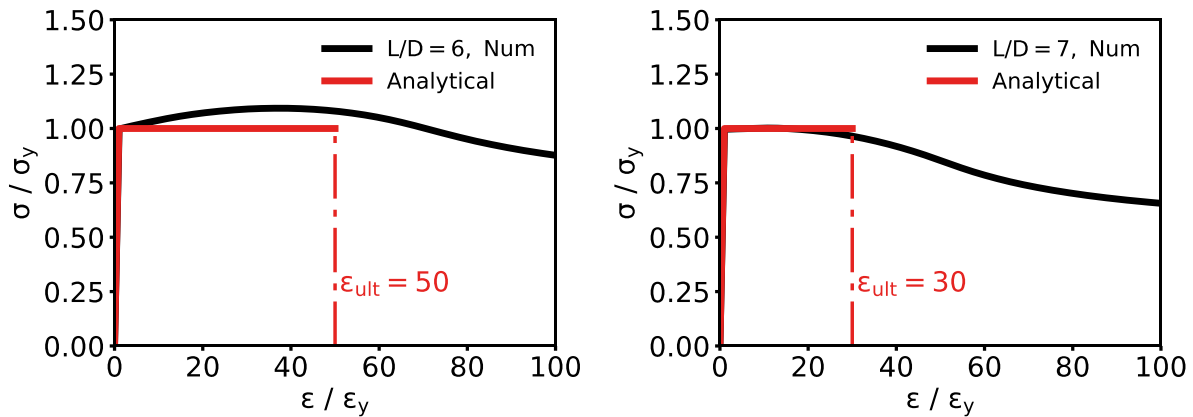
Figure 18 show the results of the numerical FE simulation for low values of slenderness ratio (e.g.,  $L/D = 5, 6$  and  $7$ )

611



612  
613 Figure 18. Numerical FE simulation for low values of slenderness ratio (e.g. LD = 5, 6 and 7)

614 The instability for  $L/D$  equal to 5 occurs for large values of the strain, whereas the ductility of the  
615 longitudinal rebar is very high. Therefore, it can be assumed that the compressive response of the  
616 smooth steel bar is coincident and symmetric to the tensile behaviour. Conversely, for slenderness  
617 ratios ranging between 6 and 7, the buckling affects the global compressive response; however, the  
618 onset of buckling appears at values of  $\varepsilon/\varepsilon_y$  equal to 50 and 30, respectively (which corresponds to  
619 strains of 4.8% and 8%, respectively). As a result, the steel bar can still exhibit high ductility; thus, it  
620 can be safely assumed an elastic-perfect plastic model with a conventional ultimate strain  
621 corresponding to the onset of buckling. The softening branch could be neglected for such slenderness  
622 ratios as the steel reinforcements in RC columns are not likely to experience such high compressive  
623 strains under cyclic loading. The analytical model for the compressive response of the  $L/D$  ratios  
624 equal to 6 and 7 is given in [Figures 19](#).



625  
626 Figure 19. Analytical Model for different  $L/D$  (e.g. LD = 6, 7)  
627

628 Based on the numerical simulation of the FE model with optimized parameters, a parametric study is  
629 also conducted to analyse the compressive stress-strain response of the steel reinforcement for  
630 slenderness ratios ranging between 8 and 20. The results of the numerical simulation are given in  
631 [Figures 20](#).

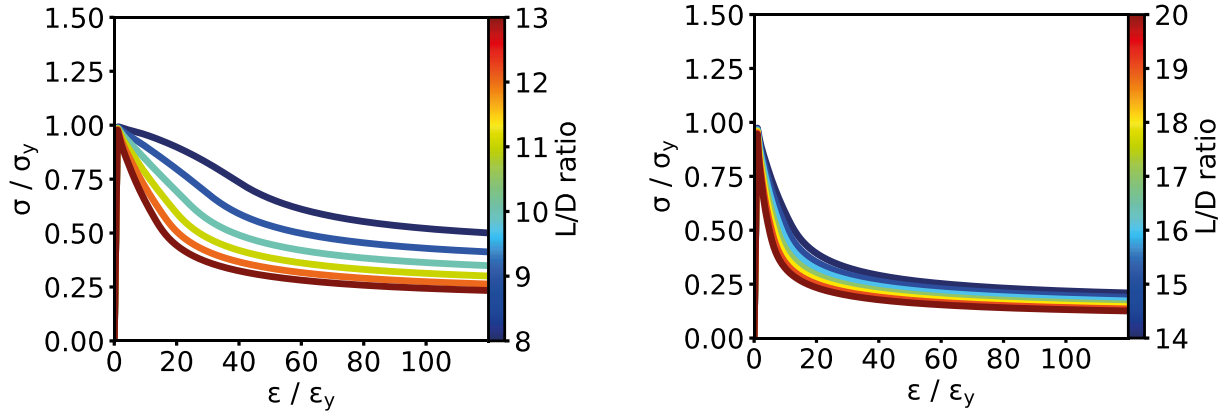


Figure 20. Numerical FE simulation for  $L/D = [8,20]$

632  
633  
634  
635  
636  
637  
638  
639  
640

The numerical stress-strain responses of smooth rebars unveil that regression analysis is needed to find the best fitting curves for the beginning of buckling and the post-buckling curve.

To generalize the formulation for the best fitting curve, the equation for the onset of buckling should be written as a function of the hardening and the yielding strain of the bar itself. The following formulation (3) can be used:

**Hardening strain** 
$$\frac{\varepsilon_{bh}}{\varepsilon_y} = 1 + \left[ \left( \frac{\varepsilon_h}{\varepsilon_y} - 1 \right) f \left( \frac{L}{D} \right) \right] \quad (4)$$

641  
642  
643  
644  
645  
646

where  $\varepsilon_{bh}$  indicates the onset of buckling,  $\varepsilon_h$  the hardening strain from the tensile response and  $\varepsilon_y$  the yielding strain. The above equation (4) has two asymptotes corresponding to 1 and  $\varepsilon_h$ , for  $L/D$  equal to 20 and 8, respectively. Figure 21a depicts the regression analysis for the strain of the buckling commencement. The function of  $L/D$  follows a power law with a negative exponent.

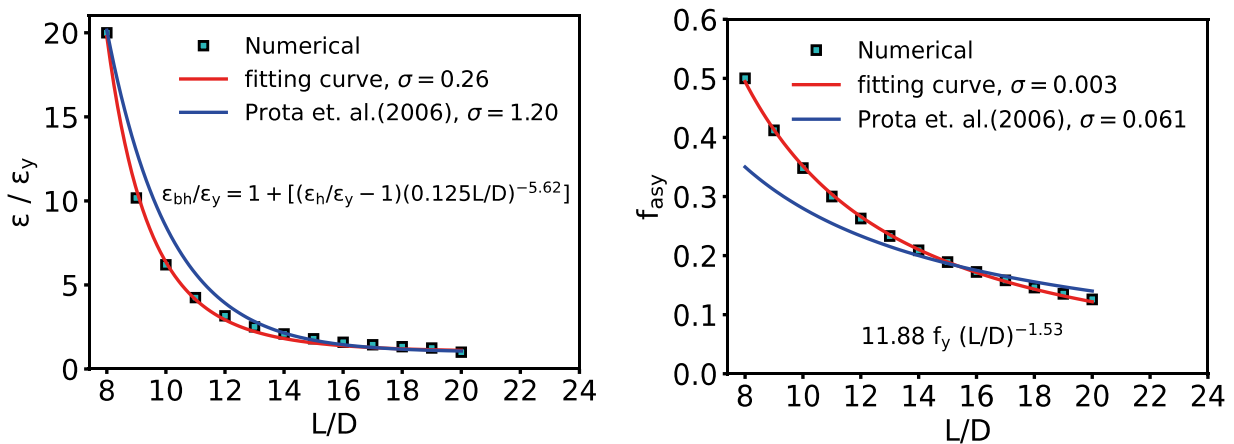


Figure 18. Regression Analysis: (a) the strain at the onset of buckling, (b) horizontal asymptote

647  
648  
649  
650  
651  
652  
653  
654

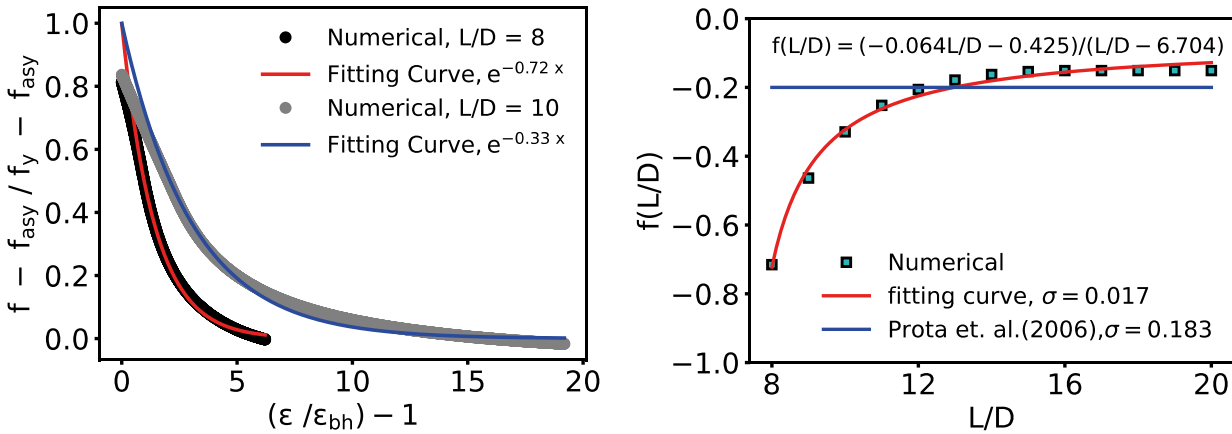
Similarly, the investigation of the post-buckling compressive response of smooth bars from the numerical parametric study indicates that all curves tend to a horizontal asymptote for infinite values of strain, while the softening curves follow a decreasing exponential function. Both trends depend on the slenderness ratio. The shape of the horizontal asymptote equation (4) can be assumed as follow:

**Asymptote** 
$$f_{asy} = \alpha f_y f\left(\frac{L}{D}\right) \tag{5}$$

655  
 656 **Figure 21b** shows the result of the regression analysis of the horizontal asymptote for different values  
 657 of the slenderness ratio (e.g.,  $L/D = [8,20]$ ).  
 658 The decreasing exponential function for the post-buckling softening depends on the ratio  $L/D$ ;  
 659 therefore, the fitting curves should follow the same exponential formulation, but different values are  
 660 expected for the regression parameters. As a result of the last observations, it is then straightforward  
 661 to formulate the post-buckling branch, as follows:  
 662

**Softening Branch** 
$$f = f_{asy} + \left[ (f_y - f_{asy}) e^{f\left(\frac{L}{D}\right)\left(\frac{\epsilon}{\epsilon_{bh}} - 1\right)} \right] \tag{6}$$

663  
 664 **Figures 22** show the regression curve for the softening branch. Since the function  $f(L/D)$  seems to  
 665 reach a constant value for large slenderness ratios, the proposed formulation for the post-buckling  
 666 softening may be used for values of  $L/D$  ratio greater than 20.



667  
 668 Figure 19. Regression Analysis for the post-buckling softening branch  
 669

670 **7.1 Validation of the analytical model**

671 In this section, the analytical model of the inelastic buckling is used to validate its accuracy against  
 672 the experimental stress-strain response of smooth rebars for different values of  $L/D$  ratios (**Figures**  
 673 **23**).

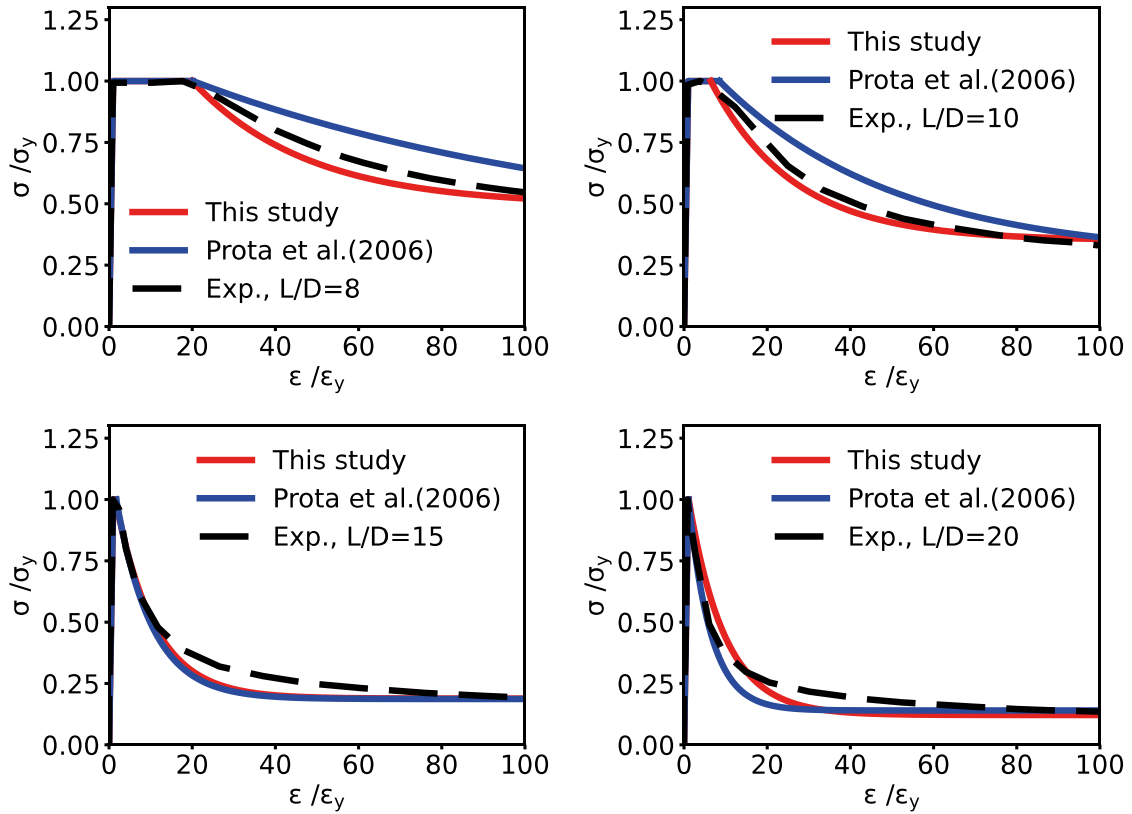


Figure 20. Analytical model vs Experimental results

674  
675  
676

Comparisons between the numerical simulations and the experimental results (Figures 23) demonstrate that the analytical model can capture the behaviour of smooth steel reinforcement under increasing monotonic compressive loading. The analytical approach seems to slightly underpredict the post-peak softening; this is mainly due to a more conservative approach when fitting the curves for larger bar slenderness values. However, the last observations do not significantly affect the global compressive response of the proposed analytical approach, which can still demonstrate an excellent agreement with the empirical tests.

684 Finally, the efficient proposed analytical model is shown in Figure 24 to represent all the theoretical monotonic curves with a slenderness ratio between 8 and 20.

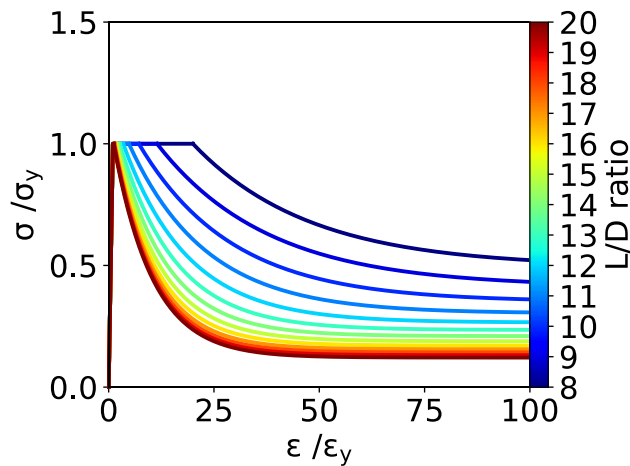


Figure 214. Analytical model for L/D ratio between 8 and 20

686  
687



688

689 Furthermore, numerical and experimental comparisons between the existing analytical model  
690 proposed by **Cosenza and Prota (2006)** and this study are presented. The results demonstrate that for  
691 values of the slenderness ratio ( $L/D$ ) greater than 15, typically the case for existing RC buildings  
692 where the spacing of the stirrups is very high, both models could predict the experimental tests with  
693 slightly conservative solutions. For values of slenderness ratio lesser than 15, that is the typical case  
694 of existing RC infrastructures (i.e., existing RC bridge), the actual study showed better prediction  
695 accuracy.

696 The analytical model is given for its implementation in structural engineering software. Nowadays,  
697 computer platforms for earthquake engineering applications provide several hysteretic materials  
698 (user-defined) for simulating the cyclic behaviour of steel reinforcement bars. Therefore, a backbone  
699 envelope curve of the analytical model provided for different slenderness ratio values is beneficial  
700 when using such hysteretic models; this allows a better definition of the moment-curvature to evaluate  
701 the inelastic behaviour in the critical zone of RC columns with smooth rebars, using either  
702 concentrated (plastic hinge) or spread plasticity. The last observation is relevant for the evaluation of  
703 the seismic capacity of existing RC structures reinforced with reinforcing plain bars.

704 It is also worth mentioning that some existing RC columns may exhibit potential rocking behaviour  
705 which could govern the deformation capacity, especially in the fixed-end rotation. However, both  
706 rocking and inelastic buckling are induced from loss of the bond strength between concrete and steel  
707 reinforcement; as a result, they depend upon both the construction details and the mechanisms of  
708 transferring the stresses in the RC components. In this case, the proposed analytical model is still  
709 beneficial as it could be coupled with approaches that account for the rocking behaviour, as a sort of  
710 structural response superposition, to establish which phenomenon is governing the deformation  
711 capacity.

712

## 713 8. CONCLUSIONS

714 In this study, inelastic buckling of smooth longitudinal rebars is addressed using genetic algorithms,  
715 Bayesian model updating, and refined finite element (FE) models. The analytic study results  
716 contribute to the use of a combination of parametric optimization and FE methods to simulate the  
717 monotonic and cyclic behaviour of smooth rebars. First insight on the implementation of three current  
718 and most adopted constitutive models of steel reinforcement, available in Opensees (i.e., Steel02,  
719 SteelMPF, and ReinforcingSteel), namely calibrated for ribbed rebars, is also presented for smooth  
720 rebars. Relationships and probabilistic distributions for the model parameters are provided for each  
721 analysed constitutive model to facilitate the stress-strain definition for users. Moreover, an analytical  
722 model has also been provided to accurately simulate the monotonic compressive response. The  
723 outcomes of this study demonstrate that:

- 724 1. The proposed optimization procedure is an efficient and robust technique that accounts for  
725 the selected steel constitutive model parameters. It accurately leads to the optimal solution  
726 with a reasonable computational cost. Notably, the pre-optimization based on few running of  
727 the FE model allows a proper estimation of pre-defined intervals of all parameters to be  
728 optimized;
- 729 2. The adopted advanced FE model for steel rebars, based on element and cross-section  
730 discretization from sensitivity analyses, provided accurate and reliable results, compared to  
731 the experimental tests, when simulating the monotonic and cyclic response of ribbed rebar

732 using default parameters. Numerical simulations for all examined steel constitutive models  
 733 show that the FE model could adequately predict the onset of buckling and the post-buckling  
 734 softening of the empirical results. Steel02 and SteelMPF demonstrated a slight  
 735 underestimation of the hardening for low values of L/D. Conversely, the ReinforcingSteel  
 736 material could also predict the yield plateau, while a small overprediction in the post-buckling  
 737 softening branch for L/D equal to 10 was noted. All materials exhibited an excellent match  
 738 with experimental results for large values of L/D ratio;

- 739 3. The joint optimization procedure could produce accurate results as the monotonic and cyclic  
 740 behaviour are entirely obtained for the full path (compression – tension). The error, referred  
 741 to the area of each half-cycle, is compatible from an engineering standpoint (or compatible  
 742 with engineering applications);
- 743 4. The hardening ratio seems not to vary for different bar slenderness values but is reduced by a  
 744 constant factor equal to 1.8, while a linear interpolation was appropriate for the isotropic  
 745 hardening and the initial curvature of the constitutive models. The homoscedastic statistic  
 746 model to apply the model updating, based on the regression analyses, further validated the  
 747 accuracy of the modelling approach accounting even for the uncertainties of the model  
 748 parameters, numerical modelling, and experimental measurement;
- 749 5. The proposed improvement of the analytical model was able to adequately predict the  
 750 compressive monotonic response of steel smooth rebars when compared to empirical results.  
 751 A slight conservative solution was shown for the post-buckling softening branch of L/D equal  
 752 to 15 and 20 without affecting the global compressive response compared to the experimental  
 753 results. For L/D equal to 8 and 10, the response was in complete agreement with empirical  
 754 tests. Compared to the existing analytical model, the actual improvement is more accurate for  
 755 a slenderness ratio lesser than 15, which typically refers to existing RC infrastructure.

756 Based on the discussion provided above, it is expected that future works should focus on the analytical  
 757 formulation of the cyclic response of smooth rebars based on different loading strain histories. Thus,  
 758 it will be possible to account reliably for the path-dependency. If other experimental results are made  
 759 available, such an approach can be extended to investigate such an issue.

#### 761 Acknowledgements

762 The authors would like to acknowledge the gracious support of this work through the EPSRC and ESRC Centre for  
 763 Doctoral Training on Quantification and Management of Risk and Uncertainty in Complex Systems Environments Grant  
 764 No. (EP/L015927/1). The third author is supported by the Engineering and Physical Sciences Research Council (EPSRC)  
 765 project UKCRIC (EP/R012806/1).  
 766

#### 767 9. References

- 769 1. **Abbiati G, Bursi OS, Caperan P, Di Sarno L, Molina FJ, Paolacci F**, et al. Hybrid simulation  
 770 of a multi-span RC viaduct with plain bars and sliding bearings. *Earthq Eng Struct Dyn* 2015.  
 771 <http://dx.doi.org/10.1002/eqe.2580>.
- 772 2. **Akkaya, Y. & Guner, S. & Vecchio, F.** (2019). Constitutive Model for Inelastic Buckling  
 773 Behavior of Reinforcing Bars. *Aci Structural Journal*. 116. 195-204. 10.14359/51711143.
- 774 3. **Arani, K. K., Di Ludovico, M., Marefat, M. S., Prota, A. and Manfredi, G.** (2014). Lateral  
 775 Response Evaluation of Old Type Reinforced Concrete Columns with Smooth Bars, *ACI*  
 776 *Structural Journal*, Vol. 111, Issue 4, doi: 10.14359/51686734

- 777 4. Arani, K.K., Marefat, M.S., Di Ludovico, M. (2013). Hysteretic cyclic response of concrete  
778 columns reinforced with smooth bars. *Bull Earthquake Eng* 11, 2033–2053 (2013).  
779 <https://doi.org/10.1007/s10518-013-9469-9>
- 780 5. ASTM A6 / A6M-19, Standard Specification for General Requirements for Rolled Structural  
781 Steel Bars, Plates, Shapes, and Sheet Piling, ASTM International, West Conshohocken, PA,  
782 2019, [www.astm.org](http://www.astm.org)
- 783 6. Bae S, Miseses A, Bayrak O. Inelastic buckling of reinforcing bars. *J Struct Eng*  
784 2005;131(2):314–21.
- 785 7. Brown, J. and Kunnath, S.K. (2000). Low Cycle Fatigue Behavior of Longitudinal  
786 Reinforcement in Reinforced Concrete Bridge Columns. NCEER Technical Report 00-0007.
- 787 8. C.A. Coello, A.D. Christiansen, Multiobjective optimization of trusses using genetic  
788 algorithms, *Computers & Structures*, Volume 75, Issue 6, 2000, Pages 647-660, ISSN 0045-  
789 7949, [https://doi.org/10.1016/S0045-7949\(99\)00110-8](https://doi.org/10.1016/S0045-7949(99)00110-8).
- 790 9. Castaldo P., Gino D., Bertagnoli G., Mancini G. (2020) Resistance model uncertainty in non-  
791 linear finite element analyses of cyclically loaded reinforced concrete systems, *Engineering*  
792 *Structures*, 211,110496
- 793 10. Castaldo P., Gino D., Mancini G. (2019) Safety formats for non-linear finite element analysis  
794 of reinforced concrete structures: discussion, comparison and proposals, *Engineering*  
795 *Structures*, 193, pp. 136-153.
- 796 11. Celarec, D., Dolšek, M. (2013) The impact of modelling uncertainties on the seismic  
797 performance assessment of reinforced concrete frame buildings, *Engineering Structures*, 52,  
798 340-354.
- 799 12. Chang, G., and Mander, J. (1994). “Seismic energy based fatigue damage analysis of bridge  
800 columns: Part I-Evaluation of seismic capacity.” NCEER Technical Rep. No. 94-0006,  
801 Buffalo, N.Y.
- 802 13. Coffin, L. F., Jr. (1971). “A note on low cycle fatigue laws.” *J. Mater.*, 6, 388–402.
- 803 14. Cosenza, E. and Prota, A. (2006). Experimental Behaviour and Numerical Modelling Of  
804 Smooth Steel Bars Under Compression, *Journal of Earthquake Engineering*, Vol. = 10,  
805 number = 3, pages = 313-329, Taylor & Francis, <https://doi.org/10.1080/13632460609350599>
- 806 15. De Risi, R., Di Sarno, L., and Paolacci, F. Probabilistic seismic performance assessment of  
807 an existing RC bridge with portal-frame piers designed for gravity loads only, *Engineering*  
808 *Structures*, Volume 145, 2017, Pages 348-367, ISSN 0141-0296,  
809 <https://doi.org/10.1016/j.engstruct.2017.04.053>.
- 810 16. Dhakal RP, Maekawa K. Modeling for postyield buckling of reinforcement. *J Struct Eng*  
811 2002;128(9):1139–47.
- 812 17. Di Sarno L, Pugliese F (2020b). Seismic fragility of existing rc buildings with corroded bars  
813 under earthquake sequences. *Soil Dynamics and Earthquake Engineering*, Volume 134, 2020,  
814 106169, ISSN 0267-7261, <https://doi.org/10.1016/j.soildyn.2020.106169>.
- 815 18. Di Sarno, L., Pugliese, F. (2020a). Numerical evaluation of the seismic performance of  
816 existing reinforced concrete buildings with corroded smooth rebars. *Bull Earthquake*  
817 *Eng* 18, 4227–4273 (2020). <https://doi.org/10.1007/s10518-020-00854-8>
- 818 19. Gardoni P, Kiureghian AD, Mosalam KM. Probabilistic capacity models and fragility  
819 estimates for reinforced concrete columns based on experimental observations. *J Eng Mech*  
820 2002;128:1024–38.
- 821 20. Gomes, A., and Appleton, J., 1997, “Nonlinear Cyclic Stress-Strain Relationship of  
822 Reinforcing Bars Including Buckling,” *Engineering Structures*, V. 19, pp. 822-826.
- 823 21. Holland, J. H. [1975]. “Adaptation in Natural and Artificial Systems,” University of Michigan  
824 Press, Ann Arbor.
- 825 22. Imperatore, S., and Rinaldi Z. (2019). Experimental behavior and analytical modeling of  
826 corroded steel rebars under compression, *Construction and Building Materials*, Volume 226,  
827 2019, Pages 126-138, ISSN 0950-0618, <https://doi.org/10.1016/j.conbuildmat.2019.07.109>.

- 828 23. **J.H. Holland (1975)** *Adaptation in Natural and Artificial Systems*, University of Michigan  
829 Press, Ann Arbor, Michigan; re-issued by MIT Press (1992).
- 830 24. **Jalayer F, Iervolino I, Manfredi G.** Structural modeling uncertainties and their influence on  
831 seismic assessment of existing RC structures. *Struct Saf* 2010;32(3):220–8.
- 832 25. **Kashani, M.M. (2017).** Size Effect on Inelastic Buckling Behavior of Accelerated Pitted  
833 Corroded Bars in Porous Media. {*Journal of Materials in Civil Engineering*}, Vol., 29, nb. 7,  
834 pg. 04017022, doi = 10.1061/(ASCE)MT.1943-5533.0001853.
- 835 26. **Kunnath, S. K.; Heo, Y.; and Mohle, J. F., 2009**, “Nonlinear Uniaxial Material Model for  
836 Reinforcing Steel Bars,” *Journal of Structural Engineering*, ASCE, V. 135, No. 4, pp. 335-  
837 343. doi: 10.1061/(ASCE)0733-9445(2009)135:4(335)
- 838 27. **L. Di Sarno, A.S. Elnashai, G. Manfredi,** Assessment of RC columns subjected to horizontal  
839 and vertical ground motions recorded during the 2009 L’Aquila (Italy) earthquake,  
840 *Engineering Structures*, Volume 33, Issue 5, 2011, Pages 1514-1535, ISSN 0141-0296,  
841 <https://doi.org/10.1016/j.engstruct.2011.01.023>.
- 842 28. **L. Di Sarno, C. Del Vecchio, G. Maddaloni, A. Prota,** Experimental response of an existing  
843 RC bridge with smooth bars and preliminary numerical simulations, *Engineering Structures*,  
844 Volume 136, 2017, Pages 355-368, ISSN 0141-0296,  
845 <https://doi.org/10.1016/j.engstruct.2017.01.052>.
- 846 29. **L. Wasserman.** *All of statistics: a concise course in statistical inference*. Springer Science &  
847 Business Media, 2013.
- 848 30. **M.A. Crisfield,** "Non-linear Finite Element Analysis of Solids and Structures, Volume 1:  
849 Essentials", Wiley, 1991.
- 850 31. **M.J. Perry, C.G. Koh, Y.S. Choo,** Modified genetic algorithm strategy for structural  
851 identification, *Computers & Structures*, Volume 84, Issues 8–9, 2006, Pages 529-540, ISSN  
852 0045-7949, <https://doi.org/10.1016/j.compstruc.2005.11.008>.
- 853 32. **Manson, S. S. (1965).** “Fatigue: A complex subject—Some simple approximations.” *Exp.*  
854 *Mech.*, 5\_7\_, 193–226.
- 855 33. **Massone, L.M., and López E.E., 2014,** “Modeling of Reinforcement Global Buckling in RC  
856 elements,” *Engineering Structures*, V. 59, pp. 484-494.
- 857 34. **MATLAB.** *Global Optimization Toolbox User’s Guide R2019a*. 2019.
- 858 35. **Mau ST, El-Mabsout M.** Inelastic buckling of reinforcing bars. *J Eng Mech* 1989;115(1):1–  
859 17.
- 860 36. **McKenna, F., Scott, M. H., and Fenves, G. L.** (2010) “Non-linear finite-element analysis  
861 software architecture using object composition.” *Journal of Computing in Civil Engineering*,  
862 24(1):95-107.
- 863 37. **Melo, J., Varum, H. and Rossetto T. (2015).** Experimental cyclic behaviour of RC columns  
864 with plain bars and proposal for Eurocode 8 formula improvement, *Engineering Structures*,  
865 Volume 88, 2015, Pages 22-36, ISSN 0141-0296,  
866 <https://doi.org/10.1016/j.engstruct.2015.01.033>.
- 867 38. **Menegotto, M., and Pinto, P. E.** (1973). “Method of analysis of cyclically loaded RC plane  
868 frames including changes in geometry and nonelastic behavior of elements under normal force  
869 and bending.” Preliminary Rep. IABSE, Zurich, 13, 15–22.
- 870 39. **Mohammad M. Kashani, Laura N. Lowes, Adam J. Crewe, Nicholas A. Alexander,** Finite  
871 element investigation of the influence of corrosion pattern on inelastic buckling and cyclic  
872 response of corroded reinforcing bars, *Engineering Structures*, Volume 75, 2014, Pages 113-  
873 125, ISSN 0141-0296, <https://doi.org/10.1016/j.engstruct.2014.05.026>.
- 874 40. **Monti, G. and Nuti, C. (1992).** Non-linear Cyclic behaviour of reinforcing bars Including  
875 buckling, *Journal of Structural Engineering* 118(12), 3268–3285.
- 876 41. **Prota, A., de Cicco, F. and Cosenza, E.** (2009) Cyclic Behavior of Smooth Steel Reinforcing  
877 Bars: Experimental Analysis and Modeling Issues. *Journal of Earthquake Engineering* 13:4,  
878 pages 500-519.

- 879 42. **R. Carreño, K. H. Lotfizadeh, J. P. Conte and J. I. Restrepo (2020)**, Material Model Parameters  
880 for the Giuffre'-Menegotto-Pinto Uniaxial Steel Stress-Strain Model, Journal of Structural  
881 Engineering, Volume, 146, Number, 2, doi = 10.1061/(ASCE)ST.1943-541X.0002505
- 882 43. **Samanta Robuschi, Jakob Sumearll, Ignasi Fernandez & Karin Lundgren (2020)**: Bond of  
883 naturally corroded, plain reinforcing bars in concrete, Structure and Infrastructure  
884 Engineering, DOI: 10.1080/15732479.2020.1768273
- 885 44. **Scott, M.H. and G.L. Fenves**. "A Krylov Subspace Accelerated Newton Algorithm:  
886 Application to Dynamic Progressive Collapse Simulation of Frames." Journal of Structural  
887 Engineering, 136(5), May 2010
- 888 45. **Souza, R.M.** Force-based finite element for large displacement inelastic analysis of frames.  
889 PhD thesis, University of California, Berkeley; 2000.
- 890 46. **Spacone E, Filippou FC, Taucer FF** (1996a). Fibre beam-column model for non-linear  
891 analysis of R/C frames. Part I: Formulation. Earthq Eng Struct D 1996; 25:711-25.
- 892 47. **Spacone E, Filippou FC, Taucer FF** (1996b). Fibre beam-column model for non-linear  
893 analysis of R/C frames. Part II: Applications. Earthq Eng Struct D 1996; 25:727-42.
- 894 48. **Uriz, P. and Mahin, S. A. (2008)**, "Toward Earthquake Resistant Design of Concentrically  
895 Braced Steel-Frame Structures", PEER report 2008/08
- 896 49. **Verderame, G. M., Fabbrocino, G. and Manfredi, G. (2008)**. Seismic response of r.c. columns  
897 with smooth reinforcement. Part II: Cyclic tests, Engineering Structures, Volume 30, Issue 9,  
898 2008, Pages 2289-2300, ISSN 0141-0296, <https://doi.org/10.1016/j.engstruct.2008.01.024>.
- 899 50. **Verderame, G. M., Fabbrocino, G. and Manfredi, G. (2008)**. Seismic response of r.c. columns  
900 with smooth reinforcement. Part I: Monotonic tests, Engineering Structures, Volume 30, Issue  
901 9, 2008, Pages 2277-2288, ISSN 0141-0296, <https://doi.org/10.1016/j.engstruct.2008.01.025>.
- 902 51. **Verderame, G.M., De Carlo, G., Ricci P., and Fabbrocino, G. (2009)**. Cyclic bond behaviour  
903 of plain bars. Part II: Analytical investigation, Construction and Building Materials, Volume  
904 23, Issue 12, 2009, Pages 3512-3522, ISSN 0950-0618,  
905 <https://doi.org/10.1016/j.conbuildmat.2009.07.001>.
- 906 52. **Verderame, G.M., Ricci P., De Carlo, G. and Manfredi, G. (2009)**. Cyclic bond behaviour of  
907 plain bars. Part I: Experimental investigation, Construction and Building Materials, Volume  
908 23, Issue 12, 2009, Pages 3499-3511, ISSN 0950-0618,  
909 <https://doi.org/10.1016/j.conbuildmat.2009.07.002>.